

Screened cluster expansions for partially ionized gases

A. Alastuey*, V. Ballenegger^{†‡}, F. Cornu[§] and Ph. A. Martin[†]

February 7, 2020

Abstract

We consider a partially ionized gas at thermal equilibrium, in the Saha regime. The system is described in terms of a quantum plasma of nuclei and electrons. In this framework, the Coulomb interaction is the source of a large variety of phenomena occurring at different scales: recombination, screening, diffraction, etc. In this paper, we derive a cluster expansion adequate for a coherent treatment of those phenomena. The expansion is obtained by combining the path integral representation of the quantum gas with familiar Mayer diagrammatics. In this formalism, graphs have a clear physical interpretation: vertices are associated with recombined chemical species, while bonds describe their mutual interactions. The diagrammatical rules account exactly for all effects in the medium. Applications to thermodynamics, van der Waals forces and dielectric versus conductive behaviour will be presented in forthcoming papers.

Key words: Ionized gases; quantum plasmas; cluster expansions; recombination; screening

1 Introduction

This paper is devoted to the construction of a cluster expansion adapted to the study of partially ionized gases. In the so-called physical picture of such gases, one considers an assembly of non relativistic point nuclei and electrons in thermal equilibrium with appropriate statistics and interacting with the Coulomb potential. That fundamental approach is to be contrasted with the chemical picture which introduces preformed chemical species as elementary constituents. At this basic level of description all characteristic phenomena of charged systems such as atomic or molecular recombination, ionization, ionic and dielectric screening originate from the sole Coulomb interaction between charges. It is notoriously difficult to treat all of them from first principles in a fully coherent way. In particular one has to deal simultaneously and without intermediate modelization with the short distance part of Coulomb potential which gives rise to chemical binding (at the scale of Bohr radius), and with its long range part responsible for collective screening effects (at the scale of the classical Debye length).

*Laboratoire de physique, École Normale Supérieure de Lyon, UMR 5672 du CNRS, 46, allée d'Italie, 69364 Lyon Cedex 07, FRANCE.

[†]Institut de Théorie des Phénomènes Physiques École Polytechnique Fédérale de Lausanne EPFL, CH-1015 Lausanne, SWITZERLAND.

[‡]Present address: Department of Chemistry, University of Cambridge, Lensfield Road, Cambridge CB2 1EW, UNITED KINGDOM, E-mail: vcb25@cam.ac.uk.

[§]Laboratoire de Physique Théorique, Université Paris-Sud, UMR 8627 du CNRS, Bâtiment 210, 91405 Orsay, FRANCE.

An important point should be stressed straight away. The very concept of atom and molecule can only make sense in a low density or moderately dense medium and at temperatures sufficiently low to be away from full ionization. This situation is captured in a scaling limit called the atomic (or molecular) limit, which is more precisely described in Section 5 in the case of the Hydrogen plasma. In that limit, one lets temperature and density tend to zero in a coupled way. Low temperature favors binding over ionization, whereas low density, by increasing the available phase space, favors dissociation. The rate at which density is reduced as the temperature tends to zero determines an energy entropy balance that selects the formation of some chemical species. In the strict limit one recovers the thermodynamical laws of mixtures of ideal substances. Thus the proper physics of partially ionized gases lies in the vicinity of the atomic limit: this defines the Saha regime for which it is of interest to provide a suitable expansion.

In the literature, there exists various attempts, within the physical picture, to derive suitable expansions at low temperature and low density. First, the effective-potential method [1] has been applied to quantum plasmas by Ebeling [2]. That first-principles approach amounts to introduce an equivalent classical system of point particles with many-body potentials which incorporate all quantum effects. Low density expansions at fixed non-zero temperature have been successfully computed [2, 3, 4], while plausible expressions for basic ingredients of the chemical picture (like effective fugacities of recombined entities) have also been proposed within that framework [3, 5]. Unfortunately, an explicit control of the contribution arising from any n -body potential ($n \geq 3$) cannot be achieved by using simple diagrammatical techniques (in most previous works, only two-body potentials are retained). Therefore, all effects related to recombination into complex entities of more than two particles, cannot be properly taken into account. Another approach [6] relies on a heuristic introduction of quantum and screening effects in classical versions of usual fugacities expansions. Roughly speaking, Boltzmann factors at short distances are replaced by their quantum counterparts, while Coulomb interactions at large distances are exponentially screened over classical Debye screening length. If that method may provide rather good quantitative results at moderate temperatures and densities [7], explicit expressions for contributions related to any phenomenon are not available. Eventually, we emphasize that many-body perturbation theory [8, 9] is not suited to the description of low temperature and low density regimes. Indeed, perturbative expansions with respect to the coupling constant (the electric charge) cannot account for recombination where interactions play a crucial non-perturbative role. Consequently, that formalism is more appropriate for dealing with fully ionized regimes, either at low temperature and high density [10], or at high temperature and low density [11, 12].

In order to circumvent the drawbacks of previous methods, we introduce the path integral representation of quantum Coulomb gases. As shown in this paper, that formalism allows us to build an expansion which fulfills all requirements for a proper description of Saha regime. In particular, collective screening effects, as well as quantum mechanics of arbitrary particle clusters, are simultaneously dealt with. For the sake of presentation simplicity, derivations are carried out for the Hydrogen plasma made with protons and electrons (see Section 2). Extensions to other quantum gases are briefly mentioned in Section 5.

The functional integral representation of quantum Coulomb gas by means of Feynman-Kac formula [13] is displayed in Section 3.1. Charges of the same kind and same statistics are collected according to the cycle decomposition of the permutation group into closed Brownian paths called charged loops [14]. In terms of those loops, statistical averages are performed according to the same rules as in classical statistical mechanics. As a

consequence, the powerful methods of Mayer graphs are available in the space of loops [15]: activities including the self-energy of a loop are associated to vertices, and bonds are usual Mayer factors of interaction between different loops. Because of the long range of the Coulomb potential, those bonds are not integrable, and one has first to resum classes of diverging graphs in order to obtain an effective potential with shorter range. Since details have already been worked out in previous works [16, 15] we merely summarize the procedure in section 3.2 for the sake of completeness. The procedure follows the familiar chain graph summation as in the classical case [17, 18, 19]. The subsequent effective potential is the quantum analogue of the Debye potential. It incorporates specific features of quantum mechanics, namely quantum statistics, short distance Gibbs weight leading to binding, as well as algebraically decaying tails due to quantum fluctuations. That effective potential is extensively studied in [20]: with its help one can define a resummed diagrammatics of prototype graphs that are free from Coulomb divergencies. The rules are the same as those of standard Abe-Meeron diagrammatics. This fugacity expansion in terms of loop prototype graphs is suited to derive, at fixed non-zero temperature, low density virial equation of state in the ionized phase [21, 22]. The small parameter is the density ρ_e of unbound electrons so that contributions of bound states (e.g. hydrogen atoms) only occur as small corrections at order ρ_e^2 .

The expansion (3.25) in terms of loop prototype graphs is not well adapted to a direct analysis of Saha regime, where recombined atoms or molecules appear with comparable densities at low temperature. The reason for this inadequacy is that Gibbs factors arising in a given prototype graph do not provide the complete set of pair interactions that would correspond to an atomic or molecular Hamiltonian. Hence each prototype graph is not in direct relation with the quantities that are naturally involved in the definitions of energies and densities of recombined entities. Then, the aim is to systematically reorganize the previous loop expansion into an expansion where clusters of charges are fully interacting and are in one to one correspondance with the possible chemical binding processes. This is the content of Section 4, where we derive the main result of the paper, namely new form (4.22) of the fugacity expansion that we call the screened cluster expansion.

The derivation is accomplished in three steps. The first one (Section 4.1) consists in collecting prototype graphs into classes such that the sum of graphs in a class builds weights of fully interacting clusters of loops. This provides Gibbs factors where all pairwise interactions between loops are present. The building rules of those coefficients are the same as those of usual Mayer coefficients in standard fugacity expansions. In fact, had one to deal with a gas of particles interacting by means of short range forces, those coefficients would simply be identical to standard Mayer coefficients written within Feynman-Kac functional integral formalism. The difference here is that loops interact with the effective potential requested by the long range of Coulomb interaction. As that effective potential itself results from chain summations, one must be careful to avoid double counting of graphs. It turns out that avoiding double counting induces residual interactions between clusters through the effective potential. If now Mayer coefficients of fully interacting clusters are interpreted as dressed activities associated with vertices and residual interactions are associated with bonds, it is nice that the resulting diagrammatics is still of Mayer type in terms of those weights and bonds: this leads to formally exact representation (4.5) of the loop density. At any non-zero temperature, each graph of (4.5) is finite since bonds and vertices are entirely constructed with the help of the effective potential.

The necessity of the second step performed in Section 4.2 is the following. As explained before, the physical range of thermodynamical parameters relevant for the description of partially ionized gases lies in the neighborhood of the atomic limit, namely for vanishing

densities and temperatures. If one lets the density tend to zero in weights of (4.5), the effective potential reduces to the bare Coulomb potential so that one faces again diverging spatial integrals. Hence one needs to introduce a further step if one wants cluster integrals to have a well defined atomic limit. In rough terms, it consists simply in a regularization procedure of divergent integrals by subtraction of non-integrable part of their integrands. This leads to the introduction of truncated weights in such a way that new weights remain integrable when screening is removed. The definition of truncated cluster weights adopted here has a remarkable property: it preserves the topological rules of Mayer diagrammatics. This leads to expansion (4.18) for the loop density. The vertices are truncated Mayer coefficients, and a bond between two clusters links every loop in one cluster to every loop in the other cluster *via* the effective potential (or its second and third power).

In a third step (Section 4.3), we introduce particle clusters. If in each graph of (4.18), we detail phase-space integrations over loop internal degrees of freedom, loop clusters give rise to particle clusters. The final step amounts to collect all contributions with the same topological structure in terms of particle clusters. Then, we obtain the so-called screened cluster expansion (4.22) for the particle density. In that diagrammatic series, the graphs G (see Fig.12) are identical to familiar Mayer graphs with particle clusters in place of one-particle points. The internal state of a cluster is determined by a distribution of its particles into a given set of loops. Its statistical weight reduces to the truncated Mayer coefficient for that loop configuration. Two clusters are connected by at most one bond, which can be either the total screened interaction between the respective two sets of particles, or the square or the cube of that potential. The topological rules are usual Mayer rules, except for some specific rules that avoid double counting (see Section 4.4). Screened cluster expansions for other equilibrium quantities are discussed in Section 4.5. In particular, formula (4.31) allows one to study particle correlations.

As detailed in Section 5, screened cluster expansions do incorporate physics required for treating Saha regime. All Coulomb divergencies are removed *via* the introduction of screened interactions with proper quantum fluctuations. Recombination into complex entities is accounted for by particle clusters, because truncated Mayer coefficients do preserve the non-perturbative structure of genuine Gibbs operators with respect to interactions on one hand, while summation over all associated loop configurations restore correct Fermi symmetrization on another hand. Moreover, since the screened interaction is close to the bare Coulomb potential at short distances, familiar chemical species defined in the vacuum do emerge, for instance atoms H , molecules H_2 , ions H^- and H_2^+ , etc... Statistical weights of particle clusters are in correspondance with the densities of the associated chemical species formed by recombination of N_p protons and N_e electrons. Such weights incorporate thermal excitations, thermal and pressure dissociation, as well as spectral broadening of energy levels by collective effects. Bonds between clusters describe all possible interactions between substances present in the gas.

The present paper is merely devoted to the presentation of the general formalism. In Section 5, we also discuss a few possible applications. In forthcoming papers, we shall treat quantitatively several physical situations of interest, in particular non ideal contributions to Saha equation of state [23], the dielectric response of an atomic hydrogen gas [24] and van der Waals forces in a partially recombined plasma [25].

2 The Hydrogen plasma

2.1 Definition of the model

We consider the two-component system (in three dimensions) made of protons and electrons. In the present non-relativistic limit, the proton and the electron are viewed as quantum point particles with respective masses, charges and spins, $e_p = e$ and $e_e = -e$, m_p and m_e , $\sigma_p = 1/2$ and $\sigma_e = 1/2$. The kinetic energy operator for each particle of species $\alpha = p, e$ with position \mathbf{x} takes the Schrodinger form $-\frac{\hbar^2}{2m_\alpha}\Delta$ where Δ is the Laplacian with respect to \mathbf{x} . Two particles separated by a distance r interact via the instantaneous Coulomb potential $v(r) = 1/r$. The corresponding Coulomb Hamiltonian H_{N_p, N_e} for N_p protons and N_e electrons reads

$$H_{N_p, N_e} = - \sum_{i=1}^N \frac{\hbar^2}{2m_{\alpha_i}} \Delta_i + \frac{1}{2} \sum_{i \neq j} e_{\alpha_i} e_{\alpha_j} v(|\mathbf{x}_i - \mathbf{x}_j|) \quad (2.1)$$

where $N = N_p + N_e$ is the total number of particles. In (2.1), the subscript i is attached to protons for $i = 1, \dots, N_p$ and to electrons for $i = N_p + 1, \dots, N_p + N_e$, so the species index α_i reduces either to p or e while \mathbf{x}_i denotes either the position \mathbf{R}_i of the i -th proton or the position \mathbf{r}_j of the j -th electron ($j = i - N_p$).

The system is enclosed in a box with volume Λ , in contact with a thermostat at temperature T and a reservoir of particles that fixes the chemical potentials equal to μ_p and μ_e for protons and electrons respectively. Its grand-partition function Ξ is ($\beta = 1/(k_B T)$)

$$\Xi = \text{Tr} \exp \left[-\beta (H_{N_p, N_e} - \mu_p N_p - \mu_e N_e) \right]. \quad (2.2)$$

In (2.2), the trace is taken over all states symmetrized according to the Fermionic nature of each species; the boundary conditions for the wave functions at the surface of the box can be chosen of the Dirichlet type. Lieb and Lebowitz [26] have proved that the thermodynamic limit ($\Lambda \rightarrow \infty$ at fixed β and μ_α) exists, thanks to Fermi statistics and screening. Indeed, the Fermionic statistics of at least one species implies the H -stability [27]

$$H_{N_p, N_e} > -B(N_p + N_e), \quad B > 0 \quad (2.3)$$

that prevents the collapse of the system. On the other hand, screening ensures that it does not explode. In a fluid phase, the infinite system maintains local neutrality, i.e. the homogeneous local particle densities ρ_p and ρ_e for protons and electrons remain equal for any choice of the chemical potentials μ_α . In other words, the common particle density $\rho = \rho_p = \rho_e$, as well as all other bulk equilibrium quantities, depend on the sole combination

$$\mu = (\mu_p + \mu_e)/2, \quad (2.4)$$

and not on the difference $\nu = (\mu_e - \mu_p)/2$. In particular, in terms of the fugacities $z_\alpha = \exp(\beta\mu_\alpha)$, this means that both the density ρ and the pressure P are functions of β and $z = (z_p z_e)^{1/2} = \exp(\beta\mu)$ only. In the following, we set

$$\mu_p = \mu - \frac{3}{2} k_B T \ln \frac{\lambda_e}{\lambda_p}, \quad \mu_e = \mu + \frac{3}{2} k_B T \ln \frac{\lambda_e}{\lambda_p} \quad (2.5)$$

where $\lambda_\alpha = (\beta\hbar^2/m_\alpha)^{1/2}$ is the thermal de Broglie wavelength of species α . This choice guarantees that the Maxwell-Boltzmann densities $\rho_p^{id} = 2z_p/(2\pi\lambda_p^2)^{3/2}$ and $\rho_e^{id} = 2z_e/(2\pi\lambda_e^2)^{3/2}$

of free (no interactions) proton and electron gases respectively, are identical, i.e. $\rho_p^{id} = \rho_e^{id} = 2z/(2\pi\lambda^2)^{3/2}$ with $\lambda = (\lambda_p\lambda_e)^{1/2}$. The enforced neutrality

$$\sum_{\alpha} e_{\alpha} z_{\alpha} / (2\pi\lambda_{\alpha}^2)^{3/2} = 0 \quad (2.6)$$

of the ideal mixture simplifies the analysis of the screened cluster expansions for the interacting system derived in Section 4.

2.2 Formal Mayer expansions

For describing dilute regimes at low fugacities ($z \ll 1$), Mayer fugacity expansions are *a priori* well appropriate. That expansion for the pressure is easily inferred, at a formal level, from identity

$$\beta P = \frac{\ln \Xi}{\Lambda}, \quad (2.7)$$

where it is understood that thermodynamic limit $\Lambda \rightarrow \infty$ is taken once for all. They read

$$\beta P = \sum_{(N_p, N_e) \neq (0,0)} \frac{z_p^{N_p} z_e^{N_e}}{N_p! N_e!} B_{N_p, N_e} \quad (2.8)$$

where Mayer coefficients B_{N_p, N_e} can be expressed as suitable traces,

$$B_{N_p, N_e} = \frac{1}{\Lambda} \text{Tr} [\exp(-\beta H_{N_p, N_e})]_{\text{Mayer}}. \quad (2.9)$$

The first Mayer operators $[\exp(-\beta H_{N_p, N_e})]_{\text{Mayer}}$ read

$$\begin{aligned} [\exp(-\beta H_{1,0})]_{\text{Mayer}} &= \exp(-\beta H_{1,0}), & [\exp(-\beta H_{0,1})]_{\text{Mayer}} &= \exp(-\beta H_{0,1}), \\ [\exp(-\beta H_{1,1})]_{\text{Mayer}} &= \exp(-\beta H_{1,1}) - \exp(-\beta H_{1,0}) \exp(-\beta H_{0,1}), \end{aligned} \quad (2.10)$$

while similar expressions can be obtained for $[\exp(-\beta H_{N_p, N_e})]_{\text{Mayer}}$ by considering all possible partitions of N_p protons and N_e electrons. The traces (2.9) must be taken over symmetrized states according to Fermi statistics: for each product of Gibbs operators $\exp(-\beta H_{M_p, M_e})$ ($M_p \leq N_p$, $M_e \leq N_e$) in $[\exp(-\beta H_{N_p, N_e})]_{\text{Mayer}}$, such states are products of symmetrized states made with M_p protons and M_e electrons. For instance, in space of positions and spins, $B_{2,0}$ reads

$$\begin{aligned} B_{2,0} &= \frac{1}{\Lambda} \int d\mathbf{R}_1 \int d\mathbf{R}_2 [4 \langle \mathbf{R}_1 \mathbf{R}_2 | \exp(-\beta H_{2,0}) | \mathbf{R}_1 \mathbf{R}_2 \rangle \\ &\quad - 4 \langle \mathbf{R}_1 | \exp(-\beta H_{1,0}) | \mathbf{R}_1 \rangle \langle \mathbf{R}_2 | \exp(-\beta H_{1,0}) | \mathbf{R}_2 \rangle \\ &\quad - 2 \langle \mathbf{R}_2 \mathbf{R}_1 | \exp(-\beta H_{2,0}) | \mathbf{R}_1 \mathbf{R}_2 \rangle] \end{aligned} \quad (2.11)$$

(the prefactors 4 and 2 are due to spin degeneracy).

Mayer series for particle densities $\rho_{p,e}$, are easily obtained by inserting (2.8) into the identities

$$\rho_{\alpha} = z_{\alpha} \frac{\partial \beta P}{\partial z_{\alpha}} \quad (2.12)$$

for $\alpha = p, e$. These series read

$$\rho_p = \sum_{N_p=1, N_e=0}^{\infty} \frac{z_p^{N_p} z_e^{N_e}}{(N_p - 1)! N_e!} B_{N_p, N_e} \quad (2.13)$$

and

$$\rho_e = \sum_{N_p=0, N_e=1}^{\infty} \frac{z_p^{N_p} z_e^{N_e}}{N_p!(N_e-1)!} B_{N_p, N_e}. \quad (2.14)$$

Similar Mayer series can be derived for any equilibrium quantity. Contrary to the case of systems with short range forces, all these series must be understood in a formal sense: Mayer coefficients B_{N_p, N_e} diverge because the Coulomb potential is not integrable at large distances. The first step of our method consists in removing all Coulomb divergencies via systematic resummations of chain interactions in quantum Mayer graphs defined for an equivalent gas of classical loops (see Section 3). Then, a suitable reorganization of the resulting resummed graphs provides the required screened cluster expansion which is well suited for describing both low temperature and low fugacity regimes (see Section 4). In particular, Mayer series (2.13) are rewritten in terms of well-behaved resummed coefficients $B_{N_p, N_e}^{(R)}$, that do account for recombination into complex entities at low temperature (see Section 5).

3 Path integral formalism

Within the Feynman-Kac path integral representation, we introduce the equivalent classical gas of charged loops (section 3.1). Mayer fugacity expansions for this system are considered. We briefly sketch the resummation scheme which removes all long-range Coulomb divergencies in the Mayer graphs. This provides resummed diagrammatic expansions of the equilibrium quantities in terms of a well-behaved screened potential.

3.1 The gas of charged loops

In the definition (2.2) of the grand-partition function, the trace can be taken over symmetrized Slater sums built with one-body states $|\mathbf{x}\sigma^z\rangle$ that describe a particle localized at \mathbf{x} with the z -component of its spin equal to σ^z . This provides

$$\begin{aligned} \Xi &= \sum_{N_p, N_e=0}^{\infty} \frac{z_p^{N_p} z_e^{N_e}}{N_p! N_e!} \sum_{\mathcal{P}_p, \mathcal{P}_e} \epsilon(\mathcal{P}_p) \epsilon(\mathcal{P}_e) \sum_{\{\sigma_{p,i}^z\}, \{\sigma_{e,j}^z\}} \prod_{i=1}^{N_p} \prod_{j=1}^{N_e} \langle \sigma_{p, \mathcal{P}_p(i)}^z | \sigma_{p,i}^z \rangle \langle \sigma_{e, \mathcal{P}_e(j)}^z | \sigma_{e,j}^z \rangle \\ &\times \int_{\Lambda^N} \prod_{i=1}^{N_p} d\mathbf{R}_i \prod_{j=1}^{N_e} d\mathbf{r}_j \langle \mathbf{R}_{\mathcal{P}_p(1)} \dots \mathbf{R}_{\mathcal{P}_p(N_p)} \mathbf{r}_{\mathcal{P}_e(1)} \dots \mathbf{r}_{\mathcal{P}_e(N_e)} | \exp(-\beta H_{N_p, N_e}) | \mathbf{R}_1 \dots \mathbf{R}_{N_p} \mathbf{r}_1 \dots \mathbf{r}_{N_e} \rangle \end{aligned} \quad (3.1)$$

In (3.1), $\mathcal{P}_{p,e}$ is a permutation of $(1, \dots, N_{p,e})$, and $\epsilon(\mathcal{P}_{p,e})$ is the signature (± 1) of $\mathcal{P}_{p,e}$. Notice that the spin part of the matrix elements contributes the degeneracy factor $\sum_{\{\sigma_{p,i}^z\}, \{\sigma_{e,j}^z\}} \prod_{i=1}^{N_p} \prod_{j=1}^{N_e} \langle \sigma_{p, \mathcal{P}_p(i)}^z | \sigma_{p,i}^z \rangle \langle \sigma_{e, \mathcal{P}_e(j)}^z | \sigma_{e,j}^z \rangle$ which only depends on the permutations $\mathcal{P}_{p,e}$.

The expression (3.1) can now be transformed by using the Feynman-Kac path integral representation [13] of all diagonal and off diagonal matrix elements of $\exp(-\beta H_{N_p, N_e})$, i.e.

$$\begin{aligned} \langle \mathbf{x}'_1 \dots \mathbf{x}'_N | \exp(-\beta H_{N_p, N_e}) | \mathbf{x}_1 \dots \mathbf{x}_N \rangle &= \prod_{i=1}^N \frac{\exp[-(\mathbf{x}'_i - \mathbf{x}_i)^2 / (2\lambda_{\alpha_i}^2)]}{(2\pi\lambda_{\alpha_i}^2)^{3/2}} \int \prod_{i=1}^N \mathcal{D}(\boldsymbol{\xi}_i) \\ \exp\left[-\frac{\beta}{2} \sum_{i \neq j} e_{\alpha_i} e_{\alpha_j} \int_0^1 ds v(|(1-s)(\mathbf{x}_i - \mathbf{x}_j) + s(\mathbf{x}'_i - \mathbf{x}'_j) + \lambda_{\alpha_i} \boldsymbol{\xi}_i(s) - \lambda_{\alpha_j} \boldsymbol{\xi}_j(s)|)\right] \end{aligned} \quad (3.2)$$

In (3.2), the functional integration is carried over all Brownian bridges $\xi_i(s)$ subjected to the constraint $\xi_i(0) = \xi_i(1) = 0$, with the normalized Gaussian measure $\mathcal{D}(\xi)$ defined by its covariance

$$\int \mathcal{D}(\xi) \xi_\mu(s) \xi_\nu(t) = \delta_{\mu\nu} \inf(s, t) (1 - \sup(s, t)) \quad (3.3)$$

In the genuine formulation introduced by Feynman, $(1-s)\mathbf{x}'_i + s\mathbf{x}_i + \lambda_{\alpha_i}\xi_i(s)$ is the position of the particle i at the dimensionless time s (in units of $\beta\hbar$) along a path joining \mathbf{x}_i to \mathbf{x}'_i . If we set $\mathbf{x}'_i = \mathbf{R}_{\mathcal{P}_p(i)}$ for $i = 1, \dots, N_p$, and $\mathbf{x}'_i = \mathbf{r}_{\mathcal{P}_e(j)}$ with $j = i - N_p$ for $i = N_p + 1, \dots, Np + N_e$, we see that this path is closed if $\mathcal{P}_p(i) = i$ or $\mathcal{P}_e(j) = j$, and is open otherwise. However, since any permutation can be decomposed into a product of cyclic permutations, all open paths associated with the particles exchanged in a given cycle can be collected in a bigger closed path. Thus, as first used by Ginibre [14], Ξ then becomes identical to the grand-partition function Ξ_{loop} of a classical system of loops with Maxwell-Boltzmann statistics. The Boltzmann factor for loops was reorganized by Cornu [15] in order to exhibit a generalized loop fugacity and two-body interactions between loops. This leads to [15, 22]

$$\Xi = \Xi_{loop} = \sum_{N=0}^{\infty} \frac{1}{N!} \int \prod_{i=1}^N \mathcal{D}(\mathcal{L}_i) z(\mathcal{L}_i) \prod_{i<j} \exp(-\beta V(\mathcal{L}_i, \mathcal{L}_j)), \quad (3.4)$$

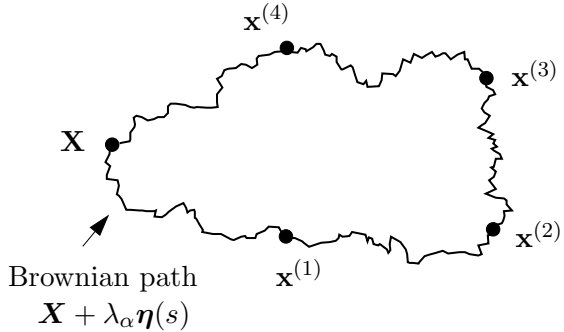
where the various symbols and quantities are defined as follows.

First, a loop \mathcal{L} is characterized by several degrees of freedom \mathbf{X} , α , q , $\eta(s)$ with $s \in [0, q]$. \mathbf{X} is the position of the loop, while α specifies the nature (electrons or protons) of the q exchanged particles in the loop. The shape of the loop $\eta(s)$ is determined by parametrizing the collection of the q trajectories followed by the q exchanged particles as $\mathbf{X} + \lambda_\alpha \eta(s)$ with $s \in [0, q]$. Within this parametrization, the genuine particle positions in the matrix elements are of the form $\mathbf{x}^{(k)} = \mathbf{X} + \lambda_\alpha \eta(k)$ with k integer, $k = 0, \dots, q-1$, and each trajectory connects $\mathbf{x}^{(k)}$ to $\mathbf{x}^{(k+1)}$ with $\mathbf{x}^{(0)} = \mathbf{x}^{(q)} = \mathbf{X}$ (see Fig.1). The closed Brownian path $\eta(s)$, $\eta(0) = \eta(q) = 0$, is distributed according to the normalized Gaussian measure $\mathcal{D}(\eta)$ with covariance

$$\int \mathcal{D}(\eta) \eta_\mu(s) \eta_\nu(t) = \delta_{\mu\nu} q \inf(s/q, t/q) (1 - \sup(s/q, t/q)). \quad (3.5)$$

In deriving (3.5), we have used that each individual trajectory is itself a Brownian path

Fig. 1 – A loop $\mathcal{L} = (\alpha, q, \mathbf{X}, \eta(s))$ made of 5 particles.



with ending points that are Gaussianly distributed. According to all the external and internal degrees of freedom which define the state of a loop, the phase-space measure

$\mathcal{D}(\mathcal{L})$ is the product of the discrete summations over α and q , the spatial integration over \mathbf{X} and the functional integration over $\boldsymbol{\eta}(s)$ with the Gaussian measure $\mathcal{D}(\boldsymbol{\eta})$, i.e.

$$\int \mathcal{D}(\mathcal{L})\dots = \sum_{\alpha=p,e} \sum_{q=1}^{\infty} \int d\mathbf{X} \int \mathcal{D}(\boldsymbol{\eta})\dots \quad (3.6)$$

The fugacity $z(\mathcal{L})$ reads [15, 22]

$$z(\mathcal{L}) = (-1)^{q-1} \frac{2}{q} \frac{z_{\alpha}^q}{(2\pi q \lambda_{\alpha}^2)^{3/2}} \exp(-\beta U(\mathcal{L})), \quad (3.7)$$

where the signature $(-1)^{q-1}$ of the cyclic permutation of the q exchanged particles accounts for Fermi statistics, the factor 2 arises from spin degeneracy, and the self energy $U(\mathcal{L})$ of the loop is

$$U(\mathcal{L}) = \frac{e^2}{2} \int_0^q ds \int_0^q dt (1 - \delta_{[s],[t]}) \tilde{\delta}(s-t) v(|\lambda_{\alpha} \boldsymbol{\eta}(s) - \lambda_{\alpha} \boldsymbol{\eta}(t)|) \quad (3.8)$$

with the Dirac comb

$$\tilde{\delta}(s-t) = \sum_{n=-\infty}^{\infty} \delta(s-t-n). \quad (3.9)$$

In (3.8), $[s]$ ($[t]$) denotes the integer part of s (t), so the factor $(1 - \delta_{[s],[t]})$ excludes the self energies of each individual particle. Eventually, the two-body potential $V(\mathcal{L}_i, \mathcal{L}_j)$ reduces to¹

$$V(\mathcal{L}_i, \mathcal{L}_j) = e_{\alpha_i} e_{\alpha_j} \int_0^q ds \int_0^q dt \tilde{\delta}(s-t) v(|\mathbf{X}_i + \lambda_{\alpha_i} \boldsymbol{\eta}_i(s) - \mathbf{X}_j - \lambda_{\alpha_j} \boldsymbol{\eta}_j(t)|). \quad (3.10)$$

In (3.10), the Dirac comb (3.9) ensures that each line element of $\boldsymbol{\eta}_i(s)$ interacts only with the corresponding line element of $\boldsymbol{\eta}_j(t)$ taken at a time t which differs from s by an integer. This “equal-time” condition can be seen as a manifestation of the quantum nature of the particles. Consequently the potential (3.10) between two loops is different from the electrostatic interaction energy between uniformly charged wires with the same shapes. This difference is the source of algebraic tails in the equilibrium correlations of quantum particles [28, 29, 30].

According to the equivalence formula (3.4), the equilibrium quantities of the quantum gas can be inferred from that of the system of loops. For instance, the particle densities ρ_{α} are related to the one-body loops density $\rho(\mathcal{L}_a)$ via the identity [15, 22],

$$\rho_{\alpha} = \sum_{q_a=1}^{\infty} \int \mathcal{D}(\boldsymbol{\eta}_a) q_a \rho(\mathcal{L}_a), \quad (3.11)$$

where α is the species index of \mathcal{L}_a .

The introduction of the gas of loops is quite useful for our purpose because the standard methods of classical statistical mechanics can be applied to this system. In particular, the equilibrium distribution functions of the loops system are formally represented by series of generalized Mayer graphs. In each graph, the usual points are now replaced by loops [15].

¹Notice that contrary to eq. (5.11) of [22], the factor $e_{\alpha_i} e_{\alpha_j}$ is here included in the definition of $V(\mathcal{L}_i, \mathcal{L}_j)$.

Each loop \mathcal{L}_i carries a statistical weight $z(\mathcal{L}_i)$. Two loops \mathcal{L}_i and \mathcal{L}_j are connected by at most one Mayer bond

$$f(\mathcal{L}_i, \mathcal{L}_j) = \exp(-\beta V(\mathcal{L}_i, \mathcal{L}_j)) - 1, \quad (3.12)$$

and the other standard topological rules [31] hold. The contribution of a given graph is obtained by integrating over all degrees of freedom of each loop, except some degrees of freedom of the root loops that define the arguments of the considered distribution function. For instance, loop density $\rho(\mathcal{L}_a)$ reads,

$$\rho(\mathcal{L}_a) = \sum_{\mathcal{G}} \frac{1}{S(\mathcal{G})} z(\mathcal{L}_a) \int \prod_n \mathcal{D}(\mathcal{L}_n) z(\mathcal{L}_n) \left[\prod f \right]_{\mathcal{G}}. \quad (3.13)$$

where the sum runs over all unlabelled topologically different connected graphs \mathcal{G} with one root point \mathcal{L}_a and $N = 0, 1, \dots$, internal points \mathcal{L}_n (for $N = 0$, the integral over the \mathcal{L}_n 's is replaced by 1). The symmetry factor $S(\mathcal{G})$ is the number of permutations of the labelled loops \mathcal{L}_n that leave the product of bonds $[\prod f]_{\mathcal{G}}$ unchanged. The first graphs that appear in (3.13) are shown in Fig.2.

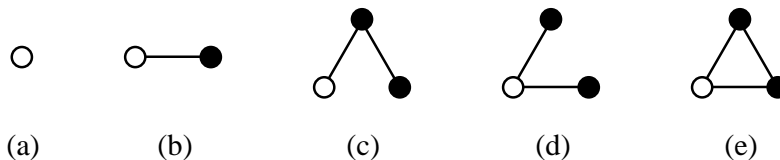


Fig. 2 – First Mayer graphs \mathcal{G} . The points stand for loops and the bonds represent Mayer factors $f = \exp(-\beta V) - 1$.

Before going further within the loop formalism, it is useful to make the connexion, at least at a formal level, between diagrammatic series (3.13) and fugacity expansions (2.13), (2.14) of particles densities $\rho_{p,e}$. First, if we sum together contributions of all graphs in (3.13) with a given number N of loops, we recover the Mayer coefficient \mathcal{B}_N that arises in the expansion of $\rho(\mathcal{L}_a)$ inferred from

$$\rho(\mathcal{L}_a) = z(\mathcal{L}_a) \frac{\delta \ln \Xi_{loop}}{\delta z(\mathcal{L}_a)}, \quad (3.14)$$

i.e.

$$\rho(\mathcal{L}_a) = \sum_{N=1}^{\infty} \frac{z(\mathcal{L}_a)}{(N-1)!} \int \prod_{i=1}^{N-1} \mathcal{D}(\mathcal{L}_i) z(\mathcal{L}_i) \mathcal{B}_N(\mathcal{L}_a, \mathcal{L}_1, \dots, \mathcal{L}_{N-1}). \quad (3.15)$$

For instance, if the graphs shown in Fig.2a. and 2b. exactly provide $\mathcal{B}_1(\mathcal{L}_a) = 1$ and

$$\mathcal{B}_2(\mathcal{L}_a, \mathcal{L}_1) = \exp(-\beta V(\mathcal{L}_a, \mathcal{L}_1)) - 1 \quad (3.16)$$

respectively, the sum of three graphs with $N = 2$ shown in Figs.2c, 2d and 2e, gives the third Mayer coefficient

$$\begin{aligned} \mathcal{B}_3(\mathcal{L}_a, \mathcal{L}_1, \mathcal{L}_2) &= \exp(-\beta V(\mathcal{L}_a, \mathcal{L}_1)) \exp(-\beta V(\mathcal{L}_a, \mathcal{L}_2)) \exp(-\beta V(\mathcal{L}_1, \mathcal{L}_2)) \\ &\quad - \exp(-\beta V(\mathcal{L}_a, \mathcal{L}_1)) - \exp(-\beta V(\mathcal{L}_a, \mathcal{L}_2)) - \exp(-\beta V(\mathcal{L}_1, \mathcal{L}_2)) + 2. \end{aligned} \quad (3.17)$$

The usual Mayer coefficients B_{N_p, N_e} that arise in expansions (2.13) and (2.14) of $\rho_{p,e}$ with respect to z_p and z_e can be recovered by inserting (3.15) into the r.h.s. of (3.11). After expressing integrations over loops degrees of freedom in terms of that of particles, we obtain each coefficient B_{N_p, N_e} by collecting together all contributions with given numbers N_p and N_e of protons and electrons respectively. The expression of B_{N_p, N_e} in terms of the suitably symmetrized traces (2.9) then follows by applying backwards the Feynman-Kac formula (3.2).

As mentioned in Section 2.2, all coefficients B_{N_p, N_e} diverge. Of course, such divergencies are still present in the Mayer graphs \mathcal{G} . In fact, since the two-body loop interactions (3.10) are long-ranged and decay as the genuine Coulomb interactions between point charges,

$$V(\mathcal{L}_i, \mathcal{L}_j) \sim \frac{q_i e_{\alpha_i} q_j e_{\alpha_j}}{|\mathbf{X}_i - \mathbf{X}_j|}, \quad |\mathbf{X}_i - \mathbf{X}_j| \rightarrow \infty, \quad (3.18)$$

the spatial integrals over the relative distances $|\mathbf{X}_i - \mathbf{X}_j|$ between different loops do not converge. Such long-range divergencies are easily removed by taking advantage of the classical nature of the loops degrees of freedom. The corresponding method is a straightforward extension [16, 15] of chain resummations introduced for classical point charges [17, 18, 19]. It is briefly sketched in the next section where we give the resummed form of the low-fugacity diagrammatic series (3.13) for $\rho(\mathcal{L}_a)$.

3.2 Resummed low-fugacity expansions

The basic trick which allows us to remove the long-range divergencies consists in the resummation of the simple convolution chains built with the long-range part of the Mayer bond. The corresponding resummations can be carried out in various ways, according to different possible decompositions of the Mayer bond. For our purpose, it is quite convenient to make the following choice [20],

$$f(\mathcal{L}_i, \mathcal{L}_j) = f_T(\mathcal{L}_i, \mathcal{L}_j) - \beta V(\mathcal{L}_i, \mathcal{L}_j) + \frac{\beta^2}{2} [V(\mathcal{L}_i, \mathcal{L}_j)]^2, \quad (3.19)$$

which defines $f_T(\mathcal{L}_i, \mathcal{L}_j)$. The replacement of each Mayer bond by its decomposition (3.19) provides new graphs built with three kinds of bonds, f_T , $-\beta V$ and $\beta^2 V^2/2$. Then, all simple convolution chains built with bonds $-\beta V$ can be resummed in terms of the sole screened potential

$$\begin{aligned} \phi(\mathcal{L}_i, \mathcal{L}_j) &= V(\mathcal{L}_i, \mathcal{L}_j) + \sum_{n=1}^{\infty} (-1)^n \beta^n \\ &\quad \times \int \left[\prod_{l=1}^n \mathcal{D}(\mathcal{L}_l) z(\mathcal{L}_l) \right] V(\mathcal{L}_i, \mathcal{L}_1) \dots V(\mathcal{L}_l, \mathcal{L}_{l+1}) \dots V(\mathcal{L}_n, \mathcal{L}_j) \end{aligned} \quad (3.20)$$

Once all chain resummations have been performed, the whole set of Mayer graphs \mathcal{G} is exactly transformed into a new set of prototype graphs \mathcal{G}_P built with the resummed bonds,

$$F_c = -\beta \phi \quad (3.21)$$

and

$$F_R = \exp(-\beta \phi) - 1 + \beta \phi. \quad (3.22)$$

The statistical weights $w(\mathcal{L})$ of loops are either $z(\mathcal{L})$ (bare loop), or $z(\mathcal{L})(\exp(I_R(\mathcal{L})) - 1)$ (dressed loop). I_R is the sum of all simple rings built with $-\beta V$; it is equal to

$$I_R(\mathcal{L}) = \frac{1}{2} \int \mathcal{D}(\mathcal{L}_1) z(\mathcal{L}_1) \beta V(\mathcal{L}, \mathcal{L}_1) \beta \phi(\mathcal{L}_1, \mathcal{L}) = \frac{\beta}{2} (V - \phi)(\mathcal{L}, \mathcal{L}) \quad (3.23)$$

The topological rules which define prototype graphs \mathcal{G}_P are identical to those relative to Mayer graphs \mathcal{G} , except for the following additional exclusion rules that avoid double counting. The convolution of two bonds F_c with an intermediate bare loop is forbidden. Moreover, when a bare loop is connected to the rest of the graph by a single bond, this bond is either F_c , or

$$F_R^{(T)} = F_R - \frac{\beta^2 \phi^2}{2}. \quad (3.24)$$

Eventually, the symmetry factors attached to the \mathcal{G}_P 's are defined as those of the \mathcal{G} 's. According to these rules, the whole series (3.13) is exactly transformed into

$$\rho(\mathcal{L}_a) = \sum_{\mathcal{G}_P} \frac{1}{S(\mathcal{G}_P)} w(\mathcal{L}_a) \int \prod_n \mathcal{D}(\mathcal{L}_n) w(\mathcal{L}_n) \left[\prod F \right]_{\mathcal{G}_P}, \quad (3.25)$$

where the sum runs over all unlabelled topologically different prototype graphs \mathcal{G}_P while w and F denote the various kinds of weights and bonds. The first graphs that appear in (3.25) are shown in Fig.3.

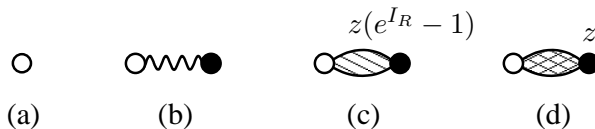


Fig. 3 – First prototype graphs \mathcal{G}_P . The possible bonds are F_c (diagram b), F_R (diagram c) and the ending bond $F_R^{(T)}$ (diagram d). If the weight of a point is not specified, it can take the two values z or $z(\exp(I_R) - 1)$.

We stress that the previous remarkably simple result follows from combinatorial and topological properties of Mayer graphs (see Appendix A). It does not depend neither on the used decomposition of the Mayer bond, nor on the specific form of the two-body potential. Therefore, the technical details of these resummations are identical to those already displayed in previous works relative to other decompositions of f [15, 32] or to relativistic interactions [33] (the corresponding proofs are simplified versions of the original derivation devised by Meeron [18] for classical point charges). The decomposition used in [15] follows by expressing the two-body loops potential V as a sum of multipolar interactions. Then, the resummations of all convolution chains built with charge-charge interactions lead to diagrammatic series analogous to (3.25). The corresponding graphs have the same topological structure as the \mathcal{G}_P 's, with different weights, bonds and exclusion rules. A brief comparison between both (equivalent) series can be found in [20].

The resummed potential ϕ is the quantum analogue of Debye potential [20]. In a dilute regime, degeneracy effects for free protons and free electrons are weak, so the classical Debye screening length $\kappa^{-1} = (4\pi\beta \sum_{\alpha} e_{\alpha}^2 \rho_{\alpha}^{id})^{-1/2} = (16\pi\beta e^2 z / (2\pi\lambda^2)^{3/2})^{-1/2}$ naturally emerges. More precisely, at large (but not infinite) distances $|\mathbf{X}_i - \mathbf{X}_j| \sim \kappa^{-1}$, $\phi(\mathcal{L}_i, \mathcal{L}_j)$

behaves as the classical Debye potential between two point charges $q_i e_{\alpha_i}$ and $q_j e_{\alpha_j}$ with screening length κ^{-1} ,

$$\phi(\mathcal{L}_i, \mathcal{L}_j) \sim q_i e_{\alpha_i} q_j e_{\alpha_j} \frac{\exp(-\kappa |\mathbf{X}_i - \mathbf{X}_j|)}{|\mathbf{X}_i - \mathbf{X}_j|}. \quad (3.26)$$

At larger distances, $|\mathbf{X}_i - \mathbf{X}_j| \gg \kappa^{-1}$, $1/|\mathbf{X}_i - \mathbf{X}_j|^3$ -dipolar interactions overcome the exponentially decaying Debye term. Out of the framework of the loops formalism, this mechanism can be seen as an irreducible manifestation of quantum mechanics that ultimately leads to algebraic tails in the particle correlations. Eventually, at short distances $|\mathbf{X}_i - \mathbf{X}_j| \ll \kappa^{-1}$, $\phi(\mathcal{L}_i, \mathcal{L}_j)$ reduces to the bare potential $V(\mathcal{L}_i, \mathcal{L}_j)$ apart from the constant $-q_i e_{\alpha_i} q_j e_{\alpha_j} \kappa$.

According to the previous properties of ϕ , both spatial and functional integrations in any prototype graph \mathcal{G}_P do converge [20]. The $1/|\mathbf{X}_i - \mathbf{X}_j|^3$ -decay of ϕ removes all long range Coulomb divergencies. Since all Coulomb singularities at the origin are smoothed out by functional integrations over shapes of loops, integrability at short distances is also fulfilled. This smearing process is nothing but the consequence of Heisenberg's uncertainty principle which prevents a quantum particle to stay at a fixed position (a similar regularization also occurs for Mayer graphs \mathcal{G} built with V). Furthermore, the exponentiated structure of Boltzmann factors, which is an essential ingredient for the description of short-range effects, is preserved through the resummation process. Indeed, both bonds F_R and $F_R^{(T)}$ provide factors $\exp(-\beta\phi)$ in the \mathcal{G}_P 's, which can be replaced by $\exp(-\beta V)$ in a dilute regime: this ensures that recombination can be properly taken into account after a suitable reorganization of prototype graphs (see Sections 4 and 5).

As a conclusion, resummed diagrammatic series (3.25) is well suited for our purpose. The resummed potential ϕ does account for classical or quantum mechanisms that prevail at either short or large distances. Here, it should be noticed that each prototype graph \mathcal{G}_P involves infinite sums over numbers q_i of particles contained in internal loops \mathcal{L}_i . Though each contribution associated with a given set $\{q_i\}$ is finite because both functional and spatial integrations converge, the discrete sum over all q_i 's may diverge [20]. Therefore, each prototype graph \mathcal{G}_P must be understood as a formal infinite collection of graphs, with identical structures in terms of loops and different particles numbers inside the loops.

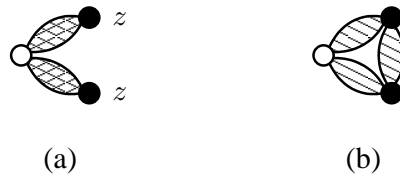
4 Resummed expansions in terms of particle clusters

In this Section, series (3.25) will be reorganized in terms of new diagrams made with finite clusters of particles. In a given cluster, all particles interact together and the weights are correctly symmetrized according to Fermi statistics. The reorganization is similar to that described in Section 3.1 for recovering the coefficients B_{N_p, N_e} from the Mayer series (3.13).

4.1 Introduction of clusters made with fully interacting loops

In each given graph \mathcal{G}_P , if we replace all bonds by their expressions in terms of ϕ , products of Boltzmann factors $\exp(-\beta\phi)$ appear. A given product of Boltzmann factors then defines a cluster of interacting loops. However, such a product may be incomplete in the sense that it does not incorporate all Boltzmann factors associated with every pair of loops. For instance, if we consider the prototype graph shown in Fig.4a, the product of bonds $\prod F = F_R^{(T)}(\mathcal{L}_a, \mathcal{L}_1) F_R^{(T)}(\mathcal{L}_a, \mathcal{L}_2)$ provides the term $\exp[-\beta\phi(\mathcal{L}_a, \mathcal{L}_1)] \exp[-\beta\phi(\mathcal{L}_a, \mathcal{L}_2)]$. This term defines the set $\{\mathcal{L}_a, \mathcal{L}_1, \mathcal{L}_2\}$ of interacting loops, and it is incomplete since the Boltzmann factor $\exp[-\beta\phi(\mathcal{L}_1, \mathcal{L}_2)]$ associated with pair $(\mathcal{L}_1, \mathcal{L}_2)$ is missing. Since all

Fig. 4 – Prototype graphs showing incomplete Boltzmann factors.



mutual interactions between particles that belong to loops $\{\mathcal{L}_a, \mathcal{L}_1, \mathcal{L}_2\}$ are not present, the considered graph provides unphysical contributions. Of course, such contributions must be cancelled out by other similar contributions arising in other graphs. In fact, if we add the contribution from graph shown in Fig.4b to that from graph in Fig.4a, we see that the previous incomplete product $\exp[-\beta\phi(\mathcal{L}_a, \mathcal{L}_1)] \exp[-\beta\phi(\mathcal{L}_a, \mathcal{L}_2)]$ does disappear. Here, we first proceed to a systematic reorganization of the whole diagrammatic series (3.25) where all incomplete products of Boltzmann factors are removed.

According to Section 3.2, graphs \mathcal{G}_P are identical to Mayer graphs of a system with ϕ in place of V and $z \exp(I_R)$ in place of z , except for some exclusion rules that avoid double counting. In the absence of such rules, the (finite) sum of graphs \mathcal{G}_P with N loops would provide the Mayer coefficient $\mathcal{B}_{\phi, N}$, similarly to the derivation of \mathcal{B}_N from the \mathcal{G} 's described in Section 3.1. Since all Boltzmann factors are complete in $\mathcal{B}_{\phi, N}$, the required reorganization would then be achieved. Here, the difficulty entirely arises from the exclusion rules which prevent to merely perform the previous sum. Our method consists in introducing parts of graphs made with M loops which are not affected by the exclusion rules, and for which summations over all possible internal structures provide the coefficient $\mathcal{B}_{\phi, M}$. The remaining parts are built with either convolutions of bonds F_c , or bonds $F_c^2/2$, so all Boltzmann factors are eventually incorporated in the $\mathcal{B}_{\phi, M}$'s.

The first step of the method is based on the introduction of new graphs \mathcal{G}_P^* defined as follows. In each graph \mathcal{G}_P , we decompose all ending bonds $F_R^{(T)}$ as F_R plus $-\beta^2\phi^2/2 = -F_c^2/2$. At the same time, we rewrite all dressed weights $z(\mathcal{L})(\exp(I_R(\mathcal{L})) - 1)$ of intermediate loops in convolutions $F_c \star F_c$ as $z(\mathcal{L}) \exp(I_R(\mathcal{L}))$ plus $-z(\mathcal{L})$. The series (3.25) then becomes

$$\rho(\mathcal{L}_a) = \sum_{\mathcal{G}_P^*} \frac{1}{S(\mathcal{G}_P^*)} w^*(\mathcal{L}_a) \int \prod_n \mathcal{D}(\mathcal{L}_n) w^*(\mathcal{L}_n) \left[\prod F^* \right]_{\mathcal{G}_P^*}. \quad (4.1)$$

The modified prototype graphs \mathcal{G}_P^* are built with three kinds of bonds F^* that are F_c , F_R or $F_c^2/2$, and four kinds of weights w^* that are z , $z(\exp(I_R) - 1)$, $z \exp(I_R)$ or $z^* = -z$. They have the same topological structure as the genuine Mayer graphs except for the following rules. The intermediate loop in a convolution $F_c \star F_c$ carries a weight which is either $z \exp(I_R)$ or z^* . Each bond $F_c^2/2$ is an ending bond that connects a single loop with weight z^* to the rest of the graph. All other loops (including the root loop \mathcal{L}_a) carry weights that are either z or $z(\exp(I_R) - 1)$. The sum in (4.1) runs over all non topologically equivalent graphs. The symmetry factor $S(\mathcal{G}_P^*)$ is defined as usual by virtue of the combinatorial properties derived in Appendix A. The first graphs \mathcal{G}_P^* are shown in Fig.5.

In each graph \mathcal{G}_P^* , we can make a partition of the ensemble of loops as follows. On one hand, there are loops with weights z^* , and on another hand, there remains all other loops which can be distributed into clusters. These clusters are defined as the remaining connected subsets when the loops with weights z^* are removed. In each cluster \mathcal{C} , bonds



Fig. 5 – First graphs \mathcal{G}_P^* . The ending bond $F_c^2/2$ is drawn as a double wavy line. As before, the points with no weight specified can take the two values z or $z \exp(I_R) - 1$.

are either F_c or F_R , and weights are either z or $z(\exp(I_R) - 1)$ except for the intermediate loops in convolutions $F_c \star F_c$ which carry weights $z \exp(I_R)$. A given loop in a cluster may be connected to another loop, in the same cluster or in another one, by convolution chains $F_c \star F_c \dots \star F_c$ where all intermediate loops carry weights z^* ; or a similar ring convolution with at least two intermediate loops can be attached to this loop. It can be also connected to ending loops with weights z^* by single bonds $F_c^2/2$. Several examples of the cluster structure of the graphs \mathcal{G}_P^* are shown in Fig.6.

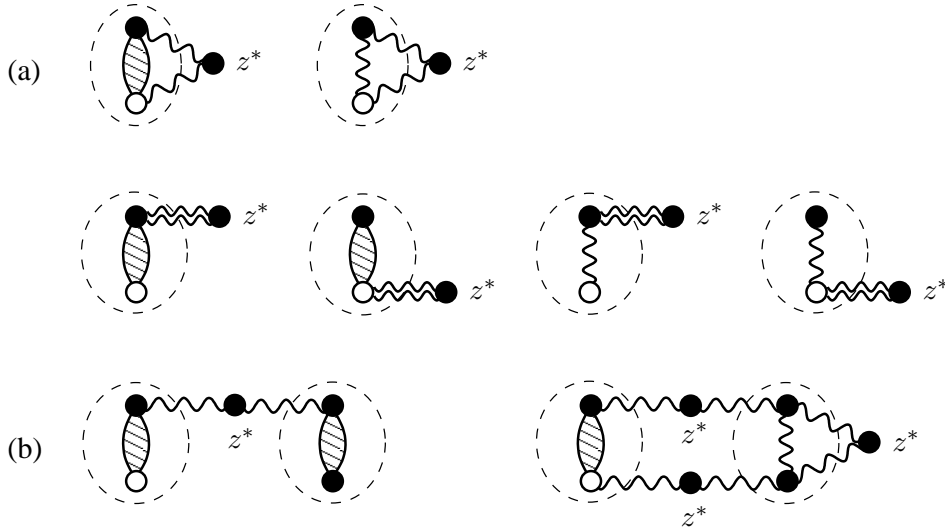


Fig. 6 – Cluster structures in the graphs \mathcal{G}_P^* . (a) graphs belonging to the same class and leading to a graph \mathcal{G}_C when added together. (b) two cluster structures belonging to different classes.

Now we proceed to a classification of graphs \mathcal{G}_P^* according to their topological structure in terms of the previous clusters and connections. All graphs in a given class have the same respective numbers of clusters and loops inside each cluster. Moreover, two loops connected by convolution chains $F_c \star F_c \dots \star F_c$ (with prescribed numbers of intermediate loops) belong to the same respective pairs of clusters, or to the same respective clusters; similarly, rings $F_c \star F_c \dots \star F_c$ (with prescribed numbers of intermediate loops) and ending bonds $F_c^2/2$ are attached to loops which belong to the same respective clusters. Various classes of graphs \mathcal{G}_P^* are shown in Fig.6. In each class, the chains can be attached to all the different loops inside a given cluster. Remember that, in such a cluster, the loops can carry any weight except z^* , and the internal bonds are F_c or F_R . Moreover, the connecting structure of convolution chains between different clusters are identical. Also, the rings or

ending bonds $F_c^2/2$ attached to single clusters are identical.

It turns out that the sum of all graphs \mathcal{G}_P in a given class can be merely rewritten as a single graph \mathcal{G}_C . Indeed, by virtue of combinatorial properties of Mayer graphs (see Appendix A), the various bonds and weights inside each respective clusters, as well as the various chains (rings) $F_c \star F_c \dots \star F_c$ and ending bonds $F_c^2/2!$, can be added together in a simultaneous and independent way. Inside each cluster, the sum of the two possible internal bonds F_c and F_R provides the Mayer bond $f_\phi = \exp(-\beta\phi) - 1$ associated with ϕ , while the corresponding sum of weights reduces to $z_\phi = z \exp(I_R)$. The further summation of all possible internal structures is analogous to that performed when relating usual Mayer graphs to Mayer coefficients (see Section 3.1). The corresponding final statistical weight $W_\phi(\mathcal{C})$ for a cluster $\mathcal{C} = \mathcal{L}_1, \dots, \mathcal{L}_N$ made with N loops reads

$$W_\phi(\mathcal{C}) = \frac{\prod_{\mathcal{L} \in \mathcal{C}} z_\phi(\mathcal{L})}{N!} \mathcal{B}_\phi(\mathcal{C}) \quad (4.2)$$

where $\mathcal{B}_\phi(\mathcal{C}) = \mathcal{B}_{\phi,N}$ is the Mayer coefficient for the N loops inside \mathcal{C} and interacting *via* ϕ (if the root loop \mathcal{L}_a belongs to \mathcal{C} , $N!$ is replaced by $(N-1)!$). The expressions of $\mathcal{B}_{\phi,N}$ are identical to that of \mathcal{B}_N with ϕ in place of V (for instance see formulas (3.16) and (3.17) for $N=2$ and $N=3$ respectively). The previous simultaneous resummations inside each cluster also amount to sum all bonds F_c that connect loops belonging to a given cluster \mathcal{C} to a loop \mathcal{L}_i with weight z^* . Since $F_c = -\beta\phi$, this gives rise to the total potential $\Phi(\mathcal{C}, \mathcal{L}_i)$ between \mathcal{C} and \mathcal{L}_i ,

$$\Phi(\mathcal{C}, \mathcal{L}_i) = \sum_{\mathcal{L} \in \mathcal{C}} \phi(\mathcal{L}, \mathcal{L}_i), \quad (4.3)$$

while the corresponding bond \mathcal{F}_c is

$$\mathcal{F}_c = -\beta\Phi. \quad (4.4)$$

Of course, all these summations do not change the topological structure of the chains, rings and ending bonds attached to the various clusters. Eventually, the series (4.1) is exactly transformed into

$$\rho(\mathcal{L}_a) = \sum_{\mathcal{G}_C} \frac{1}{S(\mathcal{G}_C)} \int \prod_i \mathcal{D}(\mathcal{C}_i) W_\phi(\mathcal{C}_i) \int \prod_n \mathcal{D}(\mathcal{L}_n) z^*(\mathcal{L}_n) \left[\prod \mathcal{F}_c \right]_{\mathcal{G}_C} \left[\prod \frac{\mathcal{F}_c^2}{2!} \right]_{\mathcal{G}_C}. \quad (4.5)$$

The integration $\mathcal{D}(\mathcal{C}_i)$ over the phase space available to cluster \mathcal{C}_i reduces to integrations over degrees of freedom of internal loops inside \mathcal{C}_i ,

$$\mathcal{D}(\mathcal{C}_i) = \prod_{\mathcal{L} \in \mathcal{C}_i} \mathcal{D}(\mathcal{L}) \quad (4.6)$$

The root loop \mathcal{L}_a necessarily belongs to one cluster, i.e. $\mathcal{C}_a = \mathcal{C}_0$, for which the product in (4.6) only runs over all the other internal loops in \mathcal{C}_a . Each bond $\mathcal{F}_c = -\beta\Phi$ connects either, one cluster to one loop with weight z^* , or two loops with weights z^* . All these bonds are distributed into convolution chains that connect two clusters, or into rings attached to a given cluster. Each bond $\mathcal{F}_c^2/2!$ connects one cluster to one ending loop with weight z^* . The loops \mathcal{L}_n with weights $z^*(\mathcal{L}_n)$ are intermediate loops in the previous chains and rings, or ending loops (there are at least two intermediate loops in each ring). Every graph \mathcal{G}_C is connected. Two clusters may be connected by an arbitrary number of chains, while an arbitrary number of rings may be attached to each cluster. The symmetry factor $S(\mathcal{G}_C)$ is defined as the number of permutations of clusters $\{\mathcal{C}_i, i \neq 0\}$ (except the root cluster \mathcal{C}_a)

and of loops $\{\mathcal{L}_n\}$ with weights z^* , that leave the product of bonds $[\prod \mathcal{F}_c]_{\mathcal{G}_C} [\prod \mathcal{F}_c^2/2!]_{\mathcal{G}_C}$ unchanged. The considered permutations separately act on loops $\{\mathcal{L}_n\}$ with weights z^* on one hand, and on subsets of clusters with identical numbers of internal loops on another hand; permutations of internal loops inside each cluster are already accounted for by the $1/N!$ factor in the definition (4.2) of the cluster weight $W_\phi(\mathcal{C})$. Eventually, the sum in (4.5) runs over all topologically different graphs \mathcal{G}_C . The first graphs in (4.5) are shown in Fig.7.

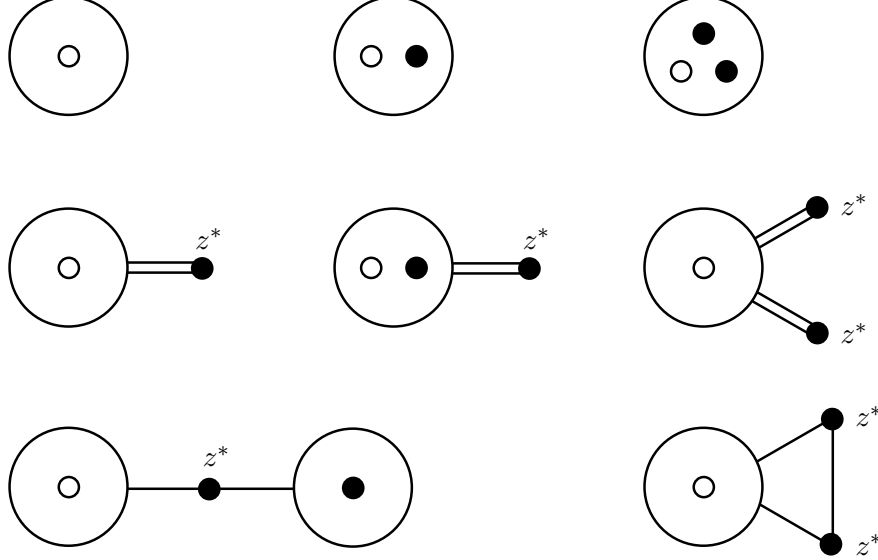


Fig. 7 – First graphs \mathcal{G}_C , corresponding to the summation of all prototype graphs made of one, two and three loops. The second graph in the second row results from the summation of the graphs (a) of Fig.6. The bond $\mathcal{F}_c(\mathcal{C}, \mathcal{L}) = -\beta\Phi(\mathcal{C}, \mathcal{L})$ between a cluster \mathcal{C} and a loop \mathcal{L} of weight z^* is drawn as a simple line, while the bond $\mathcal{F}_c^2/2!$ is drawn as a double line. The statistical weight of a cluster is $W_\phi(\mathcal{C})$.

In the diagrammatic series (4.5), the sum of all graphs \mathcal{G}_C with a single root cluster \mathcal{C}_a and no attached rings, is nothing but the density of a system of loops with potential ϕ and fugacity z_ϕ : the corresponding expression is identical to (3.15) with ϕ in place of V and z_ϕ in place of z . All the other graphs, with at least two clusters or one ring avoid double counting: they result from the exclusion rules for prototype graphs \mathcal{G}_P generated by the chain resummations where V is replaced by ϕ .

As required, each graph \mathcal{G}_C no longer involves incomplete products of Boltzmann factors $\exp(-\beta\phi)$. Indeed, all Boltzmann factors $\exp(-\beta\phi)$ are reorganized into Mayer coefficients $\mathcal{B}_\phi(\mathcal{C})$ which define the weights $W_\phi(\mathcal{C})$ of the clusters. As shown by their construction from (3.14), the \mathcal{B}_N 's involve only complete products of factors $\exp(-\beta V)$ associated with subsets of interacting loops (each product for L loops arises from the L -th order term in the expansion of Ξ_{loop} with respect to z). Of course, this property is also satisfied by the $\mathcal{B}_{\phi,N}$'s with ϕ in place of V .

4.2 Introduction of truncated Mayer coefficients

Similarly to the contribution of any prototype graph \mathcal{G}_P obtained by fixing the numbers of particles inside loops, the corresponding contributions of every graph \mathcal{G}_C are also well behaved by virtue of the sufficiently fast decay of the resummed potential ϕ . In a dilute regime, at finite distances, ϕ tends to V , so $\mathcal{B}_{\phi,N}$ can be merely replaced by \mathcal{B}_N in weights $W_\phi(\mathcal{C})$. However, this replacement is no longer legitimate for large distances between the loops inside cluster \mathcal{C} : it is crucial to keep screening effects embodied in ϕ for ensuring integrability. In order to circumvent this difficulty, we introduce truncated Mayer coefficients $\mathcal{B}_{\phi,N}^T$ such that their analogues \mathcal{B}_N^T with V in place of ϕ remain integrable at large relative distances. Of course, there are several ways of defining truncated coefficients by appropriate subtraction of terms which are not integrable when ϕ is replaced by V . The definition used below is aimed at preserving the topological structure of Mayer graphs. Indeed, within this definition, we find that the resulting diagrammatic series has a standard Mayer form in terms of the \mathcal{B}_N^T 's (see (4.18)).

Of course, no truncation is necessary for $\mathcal{B}_{\phi,1} = 1$ since there is only one loop in the associated cluster. So, we first consider $\mathcal{B}_{\phi,2}$ that is given by formula (3.16) with ϕ in place of V . We define $\mathcal{B}_{\phi,2}^T$ as

$$\mathcal{B}_{\phi,2}^T = \mathcal{B}_{\phi,2} + \beta\phi - \frac{\beta^2\phi^2}{2!} + \frac{\beta^3\phi^3}{3!}. \quad (4.7)$$

By construction, $\mathcal{B}_{\phi,2}^T$ behaves as $\beta^4\phi^4/4!$ at large distances. Therefore, $\mathcal{B}_2^T(\mathcal{L}_1, \mathcal{L}_2)$ decays as $1/|\mathbf{X}_1 - \mathbf{X}_2|^4$ when $|\mathbf{X}_1 - \mathbf{X}_2| \rightarrow \infty$, so \mathcal{B}_2^T indeed is integrable over the whole space. Notice that integrability at zero separation results from the smearing process already evocated in Section 4.2.

In order to define $\mathcal{B}_{\phi,3}^T$, we replace each Boltzmann factor $\exp(-\beta\phi)$ into $\mathcal{B}_{\phi,3}$ by

$$\exp(-\beta\phi) = 1 - \beta\phi + \frac{\beta^2\phi^2}{2!} - \frac{\beta^3\phi^3}{3!} + \mathcal{B}_{\phi,2}^T. \quad (4.8)$$

The resulting expression for $\mathcal{B}_{\phi,3}(\mathcal{L}_1, \mathcal{L}_2, \mathcal{L}_3)$ is a (finite) sum of terms that is nothing but the sum of Mayer diagrams where the Mayer bond f_ϕ has been decomposed according to (4.8). This provides various bonds g between two loops which can be either F_c , $F_c^2/2!$, $F_c^3/3!$ or $\mathcal{B}_{\phi,2}^T$. Then, $\mathcal{B}_{\phi,3}(\mathcal{L}_1, \mathcal{L}_2, \mathcal{L}_3)$ can be rewritten as

$$\mathcal{B}_{\phi,3}(\mathcal{L}_1, \mathcal{L}_2, \mathcal{L}_3) = \sum_{D_3} \left[\prod g \right]_{D_3}. \quad (4.9)$$

In (4.9), D_3 is a connected labelled diagram made with the three loops $(\mathcal{L}_1, \mathcal{L}_2, \mathcal{L}_3)$, such that two loops are connected by at most one bond g . Moreover, $[\prod g]_{D_3}$ denotes the product of bonds in D_3 , and the sum is taken over all the different diagrams (for which the products $[\prod g]_{D_3}$ are different); of course no integration is performed in D_3 over loops degrees of freedom. The truncated coefficient $\mathcal{B}_{\phi,3}^T$ is defined as the contribution to (4.9) of all diagrams which remain integrable with respect to all relative distances when ϕ is replaced by V . For diagrams which are built with bonds F_c , $F_c^2/2!$ or $F_c^3/3!$, the integrability condition is fulfilled by a simple power counting. Indeed, since V decays as $1/|\mathbf{X}_i - \mathbf{X}_j|$, the sixth-dimensional integration over the two relative distances converges if

the overall power of bonds F_c is larger than, or equal to 7. This gives

$$\begin{aligned}
\mathcal{B}_{\phi,3}^T &= \mathcal{B}_{\phi,2}^T \mathcal{B}_{\phi,2}^T \mathcal{B}_{\phi,2}^T + \sum \mathcal{B}_{\phi,2}^T \mathcal{B}_{\phi,2}^T \\
&+ \sum \mathcal{B}_{\phi,2}^T \mathcal{B}_{\phi,2}^T F_c + \sum \mathcal{B}_{\phi,2}^T \mathcal{B}_{\phi,2}^T \frac{F_c^2}{2!} + \sum \mathcal{B}_{\phi,2}^T \mathcal{B}_{\phi,2}^T \frac{F_c^3}{3!} \\
&+ \sum \mathcal{B}_{\phi,2}^T \frac{F_c^2}{2!} \frac{F_c^2}{2!} + \sum \mathcal{B}_{\phi,2}^T \frac{F_c^2}{2!} \frac{F_c^3}{3!} + \sum \mathcal{B}_{\phi,2}^T \frac{F_c^3}{3!} \frac{F_c^3}{3!} \\
&+ \sum F_c \frac{F_c^3}{3!} \frac{F_c^3}{3!} + \sum \frac{F_c^2}{2!} \frac{F_c^2}{2!} \frac{F_c^3}{3!} + \sum \frac{F_c^2}{2!} \frac{F_c^3}{3!} \frac{F_c^3}{3!} + \frac{F_c^3}{3!} \frac{F_c^3}{3!} \frac{F_c^3}{3!}, \quad (4.10)
\end{aligned}$$

where the sums run over all the (labelled) diagrams D_3 with the considered products of bonds $\mathcal{B}_{\phi,2}^T$, F_c , $F_c^2/2!$ and $F_c^3/3!$. According to this definition, we rewrite (4.9) as $\mathcal{B}_{\phi,3}^T$ plus the remaining terms that are not integrable when ϕ is replaced by V :

$$\begin{aligned}
\mathcal{B}_{\phi,3} &= \mathcal{B}_{\phi,3}^T + \sum \mathcal{B}_{\phi,2}^T F_c + \sum \mathcal{B}_{\phi,2}^T F_c F_c + \sum \mathcal{B}_{\phi,2}^T \frac{F_c^2}{2!} + \sum \mathcal{B}_{\phi,2}^T F_c \frac{F_c^2}{2!} \\
&+ \sum \mathcal{B}_{\phi,2}^T \frac{F_c^3}{3!} + \sum F_c F_c + \sum F_c \frac{F_c^2}{2!} + \sum F_c \frac{F_c^3}{3!} + \sum \frac{F_c^2}{2!} \frac{F_c^2}{2!} \\
&+ \sum \frac{F_c^2}{2!} \frac{F_c^3}{3!} + \sum \frac{F_c^3}{3!} \frac{F_c^3}{3!} + F_c F_c F_c + \sum F_c F_c \frac{F_c^2}{2!} + \sum F_c F_c \frac{F_c^3}{3!} \\
&+ \sum F_c \frac{F_c^2}{2!} \frac{F_c^3}{3!} + \sum F_c \frac{F_c^2}{2!} \frac{F_c^2}{2!} + \frac{F_c^2}{2!} \frac{F_c^2}{2!} \frac{F_c^2}{2!}. \quad (4.11)
\end{aligned}$$

The sums have the same meaning as in (4.10) in terms of diagrams D_3 .

Now we introduce new diagrams D_C by identifying clusters made with one or two loops in the diagrams D_3 : two loops are in the same cluster if they are connected by a bond $\mathcal{B}_{\phi,2}^T$. In these diagrams D_C , the loops of D_3 are replaced by the corresponding clusters. The weights of clusters with one and two loops are $\mathcal{B}_{\phi,1} = 1$ and $\mathcal{B}_{\phi,2}^T$ respectively. Two clusters are linked by at most one of the three possible bonds \mathcal{F}_c , $\mathcal{F}_c^2/2!$ or $\mathcal{F}_c^3/3!$, where \mathcal{F}_c is related to the total interaction potential Φ between the clusters, i.e. $\mathcal{F}_c = -\beta\Phi$. The total potential Φ between a cluster with two loops and a cluster with one loop is given by (4.3), while it obviously reduces to ϕ if two clusters are made with single loops. The bonds between a two-loops cluster and a one-loop cluster, result from summing together the contributions of all diagrams D_3 where the two given clusters are linked by bonds F_c for \mathcal{F}_c , by bonds $F_c F_c$ or $F_c^2/2!$ for $\mathcal{F}_c^2/2!$, by bonds $F_c F_c^2/2!$ or $F_c^3/3!$ for $\mathcal{F}_c^3/3!$. Similarly to (4.11), the resulting expression for $\mathcal{B}_{\phi,3}$ can be detailed as

$$\begin{aligned}
\mathcal{B}_{\phi,3} &= \mathcal{B}_{\phi,3}^T + \sum \mathcal{B}_{\phi,2}^T \mathcal{F}_c + \sum \mathcal{B}_{\phi,2}^T \frac{\mathcal{F}_c^2}{2!} + \sum \mathcal{B}_{\phi,2}^T \frac{\mathcal{F}_c^3}{3!} \\
&+ \sum \mathcal{F}_c \mathcal{F}_c + \sum \mathcal{F}_c \frac{\mathcal{F}_c^2}{2!} + \sum \mathcal{F}_c \frac{\mathcal{F}_c^3}{3!} + \sum \frac{\mathcal{F}_c^2}{2!} \frac{\mathcal{F}_c^2}{2!} \\
&+ \sum \frac{\mathcal{F}_c^2}{2!} \frac{\mathcal{F}_c^3}{3!} + \sum \frac{\mathcal{F}_c^3}{3!} \frac{\mathcal{F}_c^3}{3!} + \mathcal{F}_c \mathcal{F}_c \mathcal{F}_c + \sum \mathcal{F}_c \mathcal{F}_c \frac{\mathcal{F}_c^2}{2!} + \sum \mathcal{F}_c \mathcal{F}_c \frac{\mathcal{F}_c^3}{3!} \\
&+ \sum \mathcal{F}_c \frac{\mathcal{F}_c^2}{2!} \frac{\mathcal{F}_c^3}{3!} + \sum \mathcal{F}_c \frac{\mathcal{F}_c^2}{2!} \frac{\mathcal{F}_c^2}{2!} + \frac{\mathcal{F}_c^2}{2!} \frac{\mathcal{F}_c^2}{2!} \frac{\mathcal{F}_c^2}{2!}, \quad (4.12)
\end{aligned}$$

where each sum runs over all labelled diagrams D_C (loops inside a cluster are labelled) with the considered product of weights and bonds. We stress that definition (4.10) allows to introduce clusters which are connected by single bonds \mathcal{F}_c , $\mathcal{F}_c^2/2!$ or $\mathcal{F}_c^3/3!$. If $\mathcal{B}_{\phi,3}^T$ had been defined as the sum of diagrams with bonds $\mathcal{B}_{\phi,2}^T$ only (the first two terms of

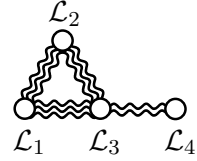
(4.10)), left-over terms in (4.10) like $\sum \mathcal{B}_{\phi,2}^T \mathcal{B}_{\phi,2}^T F_c$ or $\sum \mathcal{B}_{\phi,2}^T F_c^2/2! F_c^2/2!$, could not have been rewritten in terms of clusters connected by the sole links \mathcal{F}_c , $\mathcal{F}_c^2/2!$ or $\mathcal{F}_c^3/3!$.

The construction of the general truncated coefficient $\mathcal{B}_{\phi,N}^T$ follows from a procedure similar to that introduced above for $\mathcal{B}_{\phi,3}^T$. Each Boltzmann factor is replaced by (4.8) into $\mathcal{B}_{\phi,N}$, with the result

$$\mathcal{B}_{\phi,N} = \sum_{D_N} \left[\prod g \right]_{D_N} \quad (4.13)$$

where diagrams D_N are defined with the same rules as the D_3 's. We define $\mathcal{B}_{\phi,N}^T$ as the contribution to (4.13) of all diagrams D_N that remain integrable with respect to all relative distances when ϕ is replaced by V . For diagrams built with bonds F_c , $F_c^2/2!$ or $F_c^3/3!$, the simple power-counting rule used for $\mathcal{B}_{\phi,3}$ implies that the overall sum of powers of bonds F_c is strictly larger than $(3N - 3)$. However, for $N \geq 4$, this rule is necessary but not sufficient. For instance, the diagram shown in Fig.8 fulfills the counting rule, but it is not integrable (when ϕ is replaced by V) with respect to all separations. In fact, the determination of the integrable diagrams requires a closer analysis of their topological structure.

Fig. 8 – A diagram D_4 that fulfills the power counting rule but that is not integrable with respect to the relative distance $|\mathbf{R}_4 - \mathbf{R}_3|$ when ϕ is replaced by V . This diagram does therefore not appear in the definition of $\mathcal{B}_{\phi,4}^T$. It rather belongs to the class of graphs characterized by a F_c^2 -link between the two clusters of loops $\{\mathcal{L}_1, \mathcal{L}_2, \mathcal{L}_3\}$ and $\{\mathcal{L}_4\}$.



In each of the non-integrable diagrams, we define clusters made with M loops ($1 \leq M < N$), for which integrals over relative distances between loops inside a given cluster do converge when ϕ is replaced by V . By construction, these clusters realize a partition of the ensemble of N loops of the considered diagram D_N . As a result of this procedure, two connected clusters are linked by either one bond F_c (F_c -link), two bonds F_c or one bond $F_c^2/2!$ (F_c^2 -link), three bonds F_c , or one bond F_c and one bond $F_c^2/2!$, or one bond $F_c^3/3!$ (F_c^3 -link). A diagram D_C is defined as the sum of all diagrams D_N with identical partitions into clusters and identical structures of F_c^n -links ($1 \leq n \leq 3$) between clusters. For a given cluster made with M loops, the summation of all possible internal structures of bonds g provides, by definition, the truncated coefficient $\mathcal{B}_{\phi,M}^T$ ($\mathcal{B}_{\phi,1} = 1$ if $M = 1$). The bond \mathcal{F}_ϕ between two connected clusters, which results from the sum of all possible F_c^n -links, reduces to \mathcal{F}_c for $n = 1$, $\mathcal{F}_c^2/2!$ for $n = 2$, or $\mathcal{F}_c^3/3!$ for $n = 3$. Now, $\mathcal{F}_c = -\beta\Phi$, where Φ is the total interaction potential between two clusters, i.e.

$$\Phi(\mathcal{C}_i, \mathcal{C}_j) = \sum_{\mathcal{L}_k \in \mathcal{C}_i} \sum_{\mathcal{L}_l \in \mathcal{C}_j} \phi(\mathcal{L}_k, \mathcal{L}_l), \quad (4.14)$$

The detail of the summation leading to $\mathcal{F}_c^2/2!$ is illustrated in Fig.9.

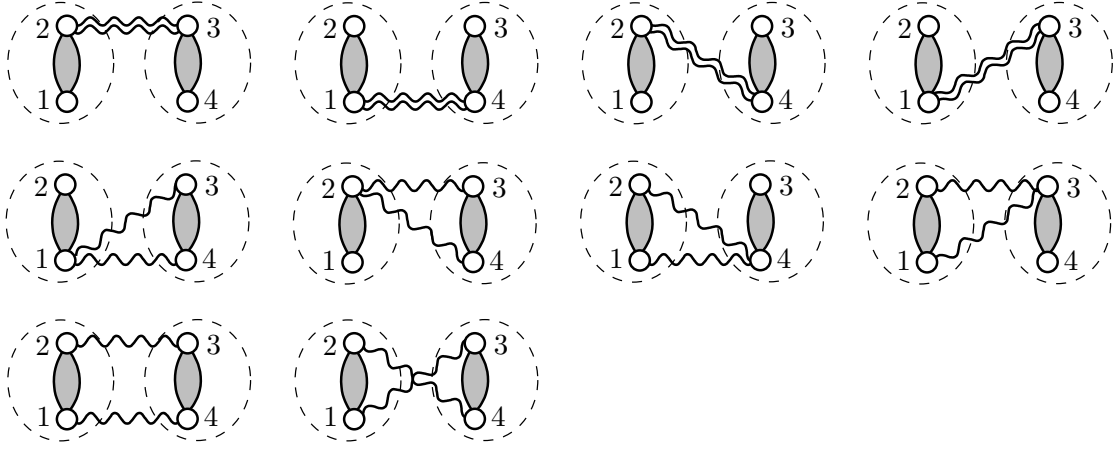


Fig. 9 – Diagrams D_4 belonging to the same class characterized by a F_c^2 -link between the two clusters of loops $\{\mathcal{L}_1, \mathcal{L}_2\}$ and $\{\mathcal{L}_3, \mathcal{L}_4\}$ (the bond $\mathcal{B}_{\phi,2}^T$ is drawn as a gray link). Their sum leads to the \mathcal{D}_C diagram $\mathcal{B}_{\phi,2}^T(\mathcal{L}_1, \mathcal{L}_2)\mathcal{B}_{\phi,2}^T(\mathcal{L}_3, \mathcal{L}_4)\mathcal{F}_c^2/2!$ in (4.15).

Therefore, similarly to formula (4.12) for $N = 3$, we can express $\mathcal{B}_{\phi,N}$ in terms of truncated coefficients as

$$\mathcal{B}_{\phi,N} = \mathcal{B}_{\phi,N}^T + \sum_{D_C} \left[\prod \mathcal{B}_{\phi,M}^T \right]_{D_C} \left[\prod \mathcal{F}_\phi \right]_{D_C}. \quad (4.15)$$

In (4.15), the sum runs over all labelled and connected diagrams D_C with at least two clusters (all M 's are strictly smaller than N), while $\left[\prod \mathcal{B}_{\phi,M}^T \right]_{D_C}$ and $\left[\prod \mathcal{F}_\phi \right]_{D_C}$ denote, respectively, the product of weights and the product of bonds for a given diagram D_C . Moreover, this sum is restricted to the diagrams which become not integrable over all relative distances between clusters when ϕ is replaced by V . For instance, in the explicit expression (4.12) of (4.15) for $N = 3$, the diagrams D_C with three one-loop clusters and products of bonds $\mathcal{F}_c \mathcal{F}_c^3/3! \mathcal{F}_c^3/3!$, $\mathcal{F}_c^2/2! \mathcal{F}_c^2/2! \mathcal{F}_c^3/3!$, $\mathcal{F}_c^2/2! \mathcal{F}_c^3/3! \mathcal{F}_c^3/3!$, or $\mathcal{F}_c^3/3! \mathcal{F}_c^3/3! \mathcal{F}_c^3/3!$, do not appear. When N increases, a detailed account of the forbidden diagrams D_C becomes rapidly cumbersome, like the explicit evaluation of the truncated coefficient $\mathcal{B}_{\phi,N}^T$ itself. However, we stress that this difficulty does not affect further diagrammatic reorganizations which are only based on the general structure of (4.15).

Now, we return to sum (4.5) over graphs \mathcal{G}_C . In each graph, we insert, into the definition (4.2) of each statistical weight $W_\phi(\mathcal{C})$, the expression (4.15) of Mayer coefficient $\mathcal{B}_\phi(\mathcal{C}) = \mathcal{B}_{\phi,N}$ for a cluster \mathcal{C} made with N loops. The whole series (4.5) is then rewritten in terms of new graphs \mathcal{G}_C^T which are still made with clusters of loops. The weight $W_\phi^T(\mathcal{C})$ of a cluster \mathcal{C} is

$$W_\phi^T(\mathcal{C}) = \frac{\prod_{\mathcal{L} \in \mathcal{C}} z_\phi(\mathcal{L})}{N!} \mathcal{B}_\phi^T(\mathcal{C}). \quad (4.16)$$

Like in (4.2), for root clusters \mathcal{C}_a which contain the root loop \mathcal{L}_a , $N!$ is replaced by $(N-1)!$ in (4.16). Two clusters are connected by at most one bond \mathcal{F} which reduces to either \mathcal{F}_c , $\mathcal{F}_c^2/2!$ or $\mathcal{F}_c^3/3!$. For any one-loop cluster $\mathcal{C} = \mathcal{L}$ which is doubly connected to the rest of the graph by two bonds \mathcal{F}_c , weight (4.16) is replaced by

$$W_\phi^T(\mathcal{L}) = z(\mathcal{L})(\exp(I_R(\mathcal{L})) - 1). \quad (4.17)$$

This specific weight results from the summation of two contributions $W_\phi(\mathcal{L}) = z_\phi(\mathcal{L}) = z(\mathcal{L}) \exp(I_R(\mathcal{L}))$ and $z^*(\mathcal{L}) = -z(\mathcal{L})$ associated respectively with a convolution $\mathcal{F}_c * \mathcal{F}_c$ in

a diagram $D_{\mathcal{C}}$, and from the same convolution in a graph $\mathcal{G}_{\mathcal{C}}$. Similarly, for a one-loop cluster $\mathcal{C} = \mathcal{L}$ which is singly connected to the rest of the graph by one bond $\mathcal{F}_c^2/2!$, the weight $W_{\phi}^T(\mathcal{L})$ also reduces to (4.17). Therefore, series (4.5) is exactly transformed into

$$\rho(\mathcal{L}_a) = \sum_{\mathcal{G}_{\mathcal{C}}^T} \frac{1}{S(\mathcal{G}_{\mathcal{C}}^T)} \int \prod_{i=0}^n \mathcal{D}(\mathcal{C}_i) W_{\phi}^T(\mathcal{C}_i) \left[\prod \mathcal{F}_{\phi} \right]_{\mathcal{G}_{\mathcal{C}}^T}, \quad (4.18)$$

where the sum runs over all unlabelled topologically different graphs $\mathcal{G}_{\mathcal{C}}^T$. Like (4.15), this sum is restricted to graphs which become not integrable with respect to the relative distances between clusters when ϕ is replaced by V . The symmetry factor $S(\mathcal{G}_{\mathcal{C}}^T)$ is the number of permutations of labelled clusters that leave the product of bonds $\left[\prod \mathcal{F}_{\phi} \right]_{\mathcal{G}_{\mathcal{C}}^T}$ unchanged (only clusters with identical numbers of loops are permuted, except the root cluster $\mathcal{C}_0 = \mathcal{C}_a$). Like in (4.5), the permutations of internal loops inside a given cluster are accounted for by the factor $1/N!$ in definition (4.16) of cluster weight $W_{\phi}^T(\mathcal{C})$. This rule follows from the same combinatorial properties (see Appendix A) that have been used in the resummation process of section 3.2 or in the construction of graphs $\mathcal{G}_{\mathcal{C}}$. Here, such properties allow us to transform the sums (4.15) over labelled clusters (with labelled internal loops) into sums over unlabelled objects. The first graphs in (4.18) are shown in Fig.10.

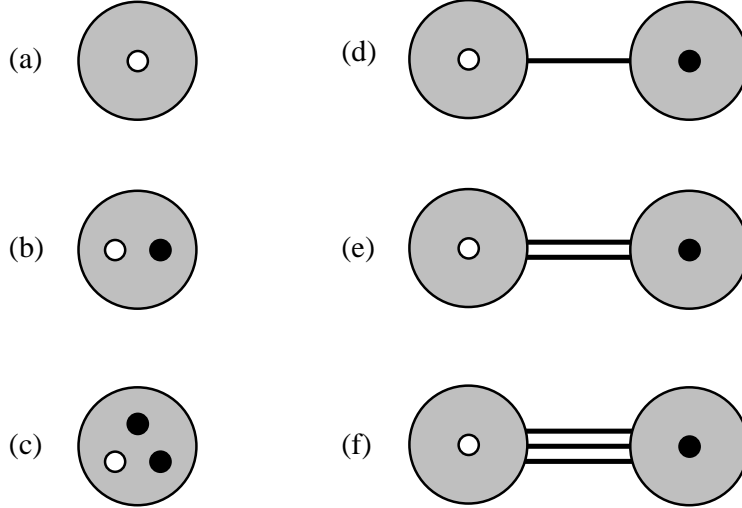


Fig. 10 – A few graphs $\mathcal{G}_{\mathcal{C}}^T$ with one or two clusters. The bonds \mathcal{F}_{ϕ} between two clusters can be either $\mathcal{F}_c = -\beta\Phi$ (single line), $\frac{1}{2!}\mathcal{F}_c^2$ (double line) or $\frac{1}{3!}\mathcal{F}_c^3$ (triple line). The small white point represents root loop \mathcal{L}_a . The clusters are drawn as shaded circles comprising a certain number of loops. The statistical weight of a cluster is given by the truncated weight $W_{\phi}^T(\mathcal{C})$ (4.16).

As required, each cluster weight $W_{\phi}^T(\mathcal{C})$ remains integrable with respect to relative distances between its internal loops when ϕ is replaced by V . Notice that products of Boltzmann factors embedded in $W_{\phi}^T(\mathcal{C})$ are complete: because of the structure of decomposition (4.15), the truncated coefficients $\mathcal{B}_{\phi,N}^T$, like the $\mathcal{B}_{\phi,N}$'s, do not involve incomplete products. Moreover, the introduction of specific weight (4.17) can be traced back to the exclusion rules for prototype graphs \mathcal{G}_P that avoid double counting.

4.3 Introduction of clusters made with particles

If we insert (4.18) into the expression (3.11) of proton density ρ_p , we find

$$\rho_p = \sum_{\mathcal{G}_C^T} \frac{1}{S(\mathcal{G}_C^T)} \sum_{q_a=1}^{\infty} \int \mathcal{D}(\mathbf{n}_a) q_a \int \prod_{i=0}^n \mathcal{D}(\mathcal{C}_i) W_{\phi}^T(\mathcal{C}_i) \left[\prod \mathcal{F}_{\phi} \right]_{\mathcal{G}_C^T}, \quad (4.19)$$

where root loop \mathcal{L}_a inside root cluster \mathcal{C}_a in each graph \mathcal{G}_C^T , is made with q_a protons. When the phase space integrations over loops inside each cluster \mathcal{C}_i are explicated, according to (3.6), in $\mathcal{D}(\mathcal{C}_i)$ given by (4.6), each graph \mathcal{G}_C^T provides an infinite sum of contributions where clusters $C(M_p, M_e)$, made with M_p protons and M_e electrons, appear. In general, in each individual contribution, the weight associated with particle cluster $C(M_p, M_e)$ is not correctly symmetrized according to Fermi statistics. For instance, the graph in Fig.10c. provides, for $(\alpha_a = p, q_a = 1; \alpha_1 = e, q_1 = 1; \alpha_2 = e, q_2 = 1)$, a cluster $C(1, 2)$ with a weight that does not include any exchange between the two electrons. However, the graph in Fig.10b also provides, for $(\alpha_a = p, q_a = 1; \alpha_1 = e, q_1 = 2)$, the same cluster $C(1, 2)$: when both contributions are summed together, Fermi symmetrization is restored. In the following, we rearrange the whole series in terms of new graphs G made with particle clusters that incorporate Fermi statistics.

Let us consider the class of graphs \mathcal{G}_C^T made with the same set of loop clusters $\{\mathcal{C}_i\}$ and the same topological connecting structure of bonds \mathcal{F}_{ϕ} . Two graphs in a given class differ by the number of internal loops in at least one cluster \mathcal{C}_i . For instance, the graphs in Figs. 10b. and 10c. belong to the same class defined by a single root cluster \mathcal{C}_a . On another hand, the graphs shown in Figs.10d., 10e. and 10f. belong to different classes because respective bonds \mathcal{F}_{ϕ} between clusters \mathcal{C}_a and \mathcal{C}_1 are different. For each cluster \mathcal{C} , specification of the nature and of the number of particles in all internal loops, leads to the introduction of a particle cluster made with N_p protons and N_e electrons. In each given class, once all graphs \mathcal{G}_C^T have been replaced by infinite sums over loop particle numbers, we sum together the contributions associated with identical sets of particle clusters $\{\mathcal{C}_i\}$ (all respective numbers $(N_i^{(p)}, N_i^{(e)})$ are identical), connected by the same bonds \mathcal{F}_{ϕ} . This defines a graph G .

In a given graph G , each particle cluster $C(N_p, N_e)$ can be traced back to a loop cluster \mathcal{C} with N loops. In the sums $\sum_{\alpha_i} \sum_{q_i}$ obtained by explicating $\mathcal{D}(\mathcal{C})$, there are several terms which can be associated with particle cluster $C(N_p, N_e)$. Each of them involves L_p protonic loops ($\alpha_i = p$) and $L_e = N - L_p$ electronic loops ($\alpha_i = e$), while the corresponding ordered sets of particles numbers, $[q_1^{(\alpha)}, \dots, q_{L_{\alpha}}^{(\alpha)}]$ with $q_1^{(\alpha)} \geq q_2^{(\alpha)} \geq \dots \geq q_{L_{\alpha}}^{(\alpha)}$, are such that

$$\sum_{k=1}^{L_{\alpha}} q_k^{(\alpha)} = N_{\alpha}. \quad (4.20)$$

The internal state of a particle cluster C then appears to be defined by the partitions $Q_{\alpha} = [q_1^{(\alpha)}, \dots, q_{L_{\alpha}}^{(\alpha)}]$ of N_{α} , and by the internal degrees of freedom of L_{α} loops with particles numbers determined by Q_{α} , L_{α} being in the range $1, \dots, N_{\alpha}$. The corresponding cluster of loops is denoted by $\mathcal{C}(Q_p, Q_e)$. An example of all possible partitions Q_{α} and clusters of loops $\mathcal{C}(Q_p, Q_e)$ associated with the same particle cluster $C(3, 2)$, are shown in Fig.11.

The statistical weight $Z_{\phi}^T(C)$ depends on internal state $(Q_p, Q_e; \mathcal{C}(Q_p, Q_e))$ of C . In the sum \sum_{α_i} arising from $\mathcal{D}(\mathcal{C})$, there are $N!/(L_p!L_e!)$ terms which define a loop cluster $\mathcal{C}(Q_p, Q_e)$ made with L_p protonic loops and L_e electronic loops. In the corresponding sum \sum_{q_i} , there are $L_p!L_e!/(\prod_{q=1}^{\infty} n_p(q)!n_e(q)!)$ terms associated with the same partitions Q_p

Particle cluster $C(3,2)$		
Q_p	Q_e	$\mathcal{C}(Q_p, Q_e)$
[3]	[2]	
[3]	[1, 1]	
[2, 1]	[2]	
[2, 1]	[1, 1]	
[1, 1, 1]	[2]	
[1, 1, 1]	[1, 1]	

Fig. 11 – The six possible partitions (Q_p, Q_e) , and the associated set of loops $\mathcal{C}(Q_p, Q_e)$, involved in the internal state of the particle cluster $C(3,2)$ made of 3 protons and 2 electrons.

and Q_e , where $n_\alpha(q)$ is the number of loops with q particles of species α . Therefore there are

$$\frac{N!}{L_p!L_e!} \times \frac{L_p!L_e!}{\prod_{q=1}^{N_p} n_p(q)! \prod_{q=1}^{N_e} n_e(q)!} = \frac{N!}{\prod_{q=1}^{\infty} n_p(q)! \prod_{q=1}^{\infty} n_e(q)!} \quad (4.21)$$

different terms in $\sum_{\alpha_i} \sum_{q_i}$ which contribute to $Z_\phi^T(C)$. Once integrations over positions and shapes of loops are performed, all these terms provide identical contributions. Thus, we define $Z_\phi^T(C)$ as the product of the number of terms (4.21) by the weight $W_\phi^T(\mathcal{C}(Q_p, Q_e))$ of loop cluster $\mathcal{C}(Q_p, Q_e)$. The phase space measure $\mathcal{D}(C)$ involves all possible internal states of $C(N_p, N_e)$: it reduces to a discrete sum over all partitions (Q_p, Q_e) satisfying the total particle number constraints (4.20), combined to spatial and functional integrations over positions and shapes of loops inside $\mathcal{C}(Q_p, Q_e)$.

The common connecting structure of graphs \mathcal{G}_C^T remains unchanged through the summations leading to graphs G . Two particle clusters C_i and C_j are connected by at most one bond \mathcal{F}_ϕ which can be either $-\beta\Phi$, $\beta^2\Phi^2/2!$, $-\beta^3\Phi^3/3!$; here Φ is the total interaction potential between two loop clusters $\mathcal{C}_i(Q_i^{(p)}, Q_i^{(e)})$ and $\mathcal{C}_j(Q_j^{(p)}, Q_j^{(e)})$ that describe internal states of C_i and C_j respectively. Again, by virtue of the combinatorial properties derived in Appendix A, $S(\mathcal{G}_C^T)$ is exactly transformed into $S(G)$ which is the number of permutations of clusters C_i (except C_a) with identical particle numbers $(N_i^{(p)}, N_i^{(e)})$ that leave the product of bonds \mathcal{F}_ϕ unchanged. Similarly to (4.19), the resulting series only involve graphs G which are no longer integrable over the relative distances between the particle clusters when ϕ is replaced by V .

4.4 The screened cluster expansion

According to section 4.3, diagrammatic series (4.19) is exactly transformed into the so called screened cluster expansion, i.e.

$$\rho_p = \sum_G \frac{1}{S(G)} \int \mathcal{D}(C_a) Z_\phi^T(C_a) q_a \int \prod_{i=1}^n \mathcal{D}(C_i) Z_\phi^T(C_i) \left[\prod \mathcal{F}_\phi \right]_G. \quad (4.22)$$

The graphs G are identical to the usual Mayer graphs, where the points are now particle clusters, except for some specific rules. The rules which define the graphs G are listed as follows:

- Every graph G involves the root cluster $C_0 = C_a$ and n ($n \geq 0$) black clusters (C_1, \dots, C_n). The root cluster C_a contains the root proton which is fixed at the origin in ρ_p . Each cluster C_i ($i = 0, \dots, n$) contains $N_i^{(p)}$ protons and $N_i^{(e)}$ electrons.
- The internal state of a cluster $C(N_p, N_e)$ ($C \in \{C_i, i = 0, \dots, n\}$) is determined, on one hand, by partitions $Q_\alpha = [q_1^{(\alpha)}, \dots, q_{L_\alpha}^{(\alpha)}]$ with $q_1^{(\alpha)} \geq q_2^{(\alpha)} \geq \dots \geq q_{L_\alpha}^{(\alpha)}$ ($\alpha = p, e$); on another hand, by loop cluster $\mathcal{C}(Q_p, Q_e)$ made with L_α loops ($\mathcal{L}_1^{(\alpha)}, \dots, \mathcal{L}_{L_\alpha}^{(\alpha)}$) where $\mathcal{L}_k^{(\alpha)}$ carries $q_k^{(\alpha)}$ particles of species α ($\alpha = p, e$). The numbers $n_\alpha(q)$ of loops carrying q particles of species α satisfy the total particle number constraints

$$\sum_{q=1}^{N_\alpha} q n_\alpha(q) = N_\alpha. \quad (4.23)$$

- The phase space measure $\mathcal{D}(C)$ for a cluster $C(N_p, N_e)$ reads

$$\mathcal{D}(C) = \sum_{Q_p, Q_e} \int \prod_{k=1}^{L_p} d\mathbf{X}_k^{(p)} \prod_{k=1}^{L_e} d\mathbf{X}_k^{(e)} \int \prod_{k=1}^{L_p} \mathcal{D}(\boldsymbol{\eta}_k^{(p)}) \prod_{k=1}^{L_e} \mathcal{D}(\boldsymbol{\eta}_k^{(e)}) \quad (4.24)$$

where $\mathbf{X}_k^{(\alpha)}$ and $\boldsymbol{\eta}_k^{(\alpha)}$ denote position and shape of loop $\mathcal{L}_k^{(\alpha)}$ respectively. The discrete sum is carried out over all partitions (Q_p, Q_e) satisfying (4.23). For root cluster C_a , loop $\mathcal{L}_1^{(p)}$ is identified to root loop \mathcal{L}_a ($q_1^{(p)} = q_a$), and no integration is performed over position $\mathbf{X}_1^{(p)} = \mathbf{X}_a$ which is fixed at the origin.

- The statistical weight $Z_\phi^T(C)$ for a cluster $C(N_p, N_e)$ reads

$$Z_\phi^T(C) = \frac{\prod_{k=1}^{L_p} z_\phi(\mathcal{L}_k^{(p)}) \prod_{k=1}^{L_e} z_\phi(\mathcal{L}_k^{(e)})}{\prod_{q=1}^{N_p} n_p(q)! \prod_{q=1}^{N_e} n_e(q)!} \mathcal{B}_\phi^T(\mathcal{C}(Q_p, Q_e)). \quad (4.25)$$

For root cluster C_a , $n_p(q_a)!$ is replaced by $(n_p(q_a) - 1)!$. For a cluster C different from C_a , the internal state of which is determined by a single protonic loop $\mathcal{L}_1^{(p)}$ or a single electronic loop $\mathcal{L}_1^{(e)}$, the expression (4.25) is replaced by ($\alpha = p, e$)

$$Z_\phi^T(C) = z_\phi(\mathcal{L}_1^{(\alpha)}) - z(\mathcal{L}_1^{(\alpha)}) \quad (4.26)$$

when C is either, the intermediate cluster of a convolution $\mathcal{F}_\phi * \mathcal{F}_\phi$, or connected to the rest of the graph by a single bond $\mathcal{F}_\phi^2/2!$. The truncated Mayer coefficient $\mathcal{B}_{\phi, N}^T$ is defined by a suitable truncation (see Section 4.2) of the usual Mayer coefficient $\mathcal{B}_{\phi, N}$ for N loops with pair interactions ϕ . This truncation ensures that $\mathcal{B}_{\phi, N}^T$ remains integrable over relative distances between loops when ϕ is replaced by V . The first truncated Mayer coefficients are

$$\mathcal{B}_{\phi, 1}^T = 1, \quad \mathcal{B}_{\phi, 2}^T = \exp(-\beta\phi) - 1 + \beta\phi - \frac{\beta^2\phi^2}{2!} + \frac{\beta^3\phi^3}{3!}, \quad \dots \quad (4.27)$$

- Two clusters C_i and C_j are connected by at most one bond $\mathcal{F}_\phi(C_i, C_j)$ which can be either $-\beta\Phi$, $\beta^2\Phi^2/2!$, $-\beta^3\Phi^3/3!$. The potential $\Phi(C_i, C_j)$ is nothing but the total interaction potential between loop clusters $\mathcal{C}_i(Q_i^{(p)}, Q_i^{(e)})$ and $\mathcal{C}_j(Q_j^{(p)}, Q_j^{(e)})$ that describe internal states of C_i and C_j respectively, i.e.

$$\Phi(C_i, C_j) = \Phi(\mathcal{C}_i, \mathcal{C}_j) = \sum_{\mathcal{L} \in \mathcal{C}_i} \sum_{\mathcal{L}' \in \mathcal{C}_j} \phi(\mathcal{L}, \mathcal{L}'). \quad (4.28)$$

The product of all bonds inside G is denoted by $\prod \mathcal{F}_\phi$. The graph G is connected, i.e. for any pair (C_i, C_j) there exists at least one connecting path made with one or more bonds \mathcal{F}_ϕ .

- The symmetry factor $S(G)$ is the number of permutations of labelled black clusters C_i ($i \geq 1$) that leave the product $\prod \mathcal{F}_\phi$ unchanged. Only clusters with identical numbers of protons and electrons are permuted.
- The sum \sum_G runs over all topologically different unlabelled graphs G which are no longer integrable over relative distances between clusters $\{C_i, i = 0, \dots, n\}$ when ϕ is replaced by V .

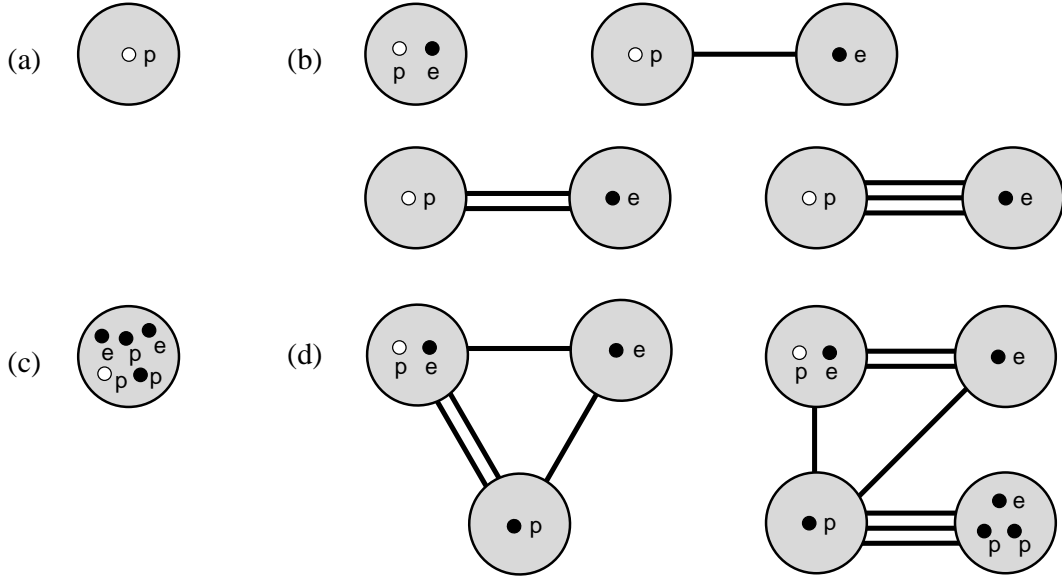


Fig. 12 – A few graphs G occurring in the screened cluster expansion of ρ_p . (a) graph made of a single proton; (b) graphs involving a proton and an electron; (c) graph consisting in the cluster $C(3,2)$, whose possible internal states are listed in Fig. 11; (d) further examples.

Several examples of graphs G are shown in Fig.12. We stress that graphs G have the same topological structure as familiar Mayer diagrams: the ordinary points are replaced by particle clusters, while usual Mayer links are now bonds \mathcal{F}_ϕ . The introduction of specific weight (4.26) avoids double counting arising from elimination of V in favor of ϕ . For a system with short range forces, a diagrammatic series similar to (4.22) can be derived without any prior chain resummations: ϕ is merely replaced by the genuine

potential, and all the above rules are conserved except that associated with specific weight (4.26). Of course, in this case, the sum of all graphs with the same number N of particles can be rewritten in terms of the sole standard Mayer coefficient of order N . Here, the (finite) sum of all graphs G_{N_p, N_e} with the same total numbers N_p of protons and N_e of electrons, provides a contribution, that can be rewritten as $(z_p^{N_p} z_e^{N_e} / (N_p - 1)! N_e!) B_{N_p, N_e}^{(R)}$ by definition of renormalized Mayer coefficient $B_{N_p, N_e}^{(R)}$. Then, screened cluster expansion (4.22) can be recast as

$$\rho_p = \sum_{N_p=1, N_e=0}^{\infty} \frac{z_p^{N_p} z_e^{N_e}}{(N_p - 1)! N_e!} B_{N_p, N_e}^{(R)}. \quad (4.29)$$

The long range divergencies which plague the bare coefficient B_{N_p, N_e} , (see Section 2.2) are removed: every graph G_{N_p, N_e} is finite because $\Phi(C_i, C_j)$ decays as a dipolar interaction for large separations between C_i and C_j . Since screened potential ϕ depends on fugacities, $B_{N_p, N_e}^{(R)}$ does not depend on the sole temperature, contrary to usual Mayer coefficients for systems with short range forces.

4.5 Particle correlations and other observables

The particle correlations, as well as other physical observables, can be inferred from multi-body loop densities. Hence, the screened cluster expansion of such physical quantities will directly follow from the expansions of these loop densities that are analogous to (4.22). In particular, by starting from (4.18) and following the same lines as in Section 4.3, we easily obtain for (one-body) loop density $\rho(\mathcal{L}_a)$

$$\rho(\mathcal{L}_a) = \sum_G \frac{1}{S(G)} \int \mathcal{D}(C_a) Z_\phi^T(C_a) \left(\sum_{\mathcal{L} \in C_a} \delta(\mathcal{L}, \mathcal{L}_a) \right) \int \prod_{i=1}^n \mathcal{D}(C_i) Z_\phi^T(C_i) \left[\prod \mathcal{F}_\phi \right]_G, \quad (4.30)$$

where graphs G are identical to those in (4.22). The sole difference between (4.30) and (4.22) lies in the integration upon degrees of freedom of root cluster C_a . Now $\mathcal{D}(C_a)$ and $Z_\phi^T(C_a)$ are also given by (4.24) and (4.25) respectively, while factor $\delta(\mathcal{L}, \mathcal{L}_a)$ selects the contribution of internal states of C_a where one loop \mathcal{L} is identified to \mathcal{L}_a . It is easily checked that series (4.22) for the protonic density can be recovered by inserting (4.30) into (3.11). Notice that factor $1/(n_p(q_a) - 1)!$ occurring in (4.22) results from the fact that there are $n_p(q_a)$ loops in (4.30) identified to \mathcal{L}_a . The screened cluster expansion of other one-body physical quantities might be also merely derived from (4.30).

The truncated two-body loop density (loop correlations), can be expanded similarly to (4.30). Its screened cluster expansion reads

$$\begin{aligned} \rho_T(\mathcal{L}_a, \mathcal{L}_b) = & \sum_G \frac{1}{S(G)} \int \mathcal{D}(C_{ab}) \left(\sum_{\mathcal{L}_k, \mathcal{L}_l \in C_{ab}, k \neq l} \delta(\mathcal{L}_k, \mathcal{L}_a) \delta(\mathcal{L}_l, \mathcal{L}_b) \right) Z_\phi^T(C_{ab}) \\ & \times \int \prod_i \mathcal{D}(C_i) Z_\phi^T(C_i) \left[\prod \mathcal{F}_\phi \right]_G + \\ & + \sum_G \frac{1}{S(G)} \int \mathcal{D}(C_a) \mathcal{D}(C_b) \left(\sum_{\mathcal{L}_k \in C_a} \delta(\mathcal{L}_k, \mathcal{L}_a) \sum_{\mathcal{L}_l \in C_b} \delta(\mathcal{L}_l, \mathcal{L}_b) \right) Z_\phi^T(C_a) Z_\phi^T(C_b) \\ & \times \int \prod_i \mathcal{D}(C_i) Z_\phi^T(C_i) \left[\prod \mathcal{F}_\phi \right]_G. \quad (4.31) \end{aligned}$$

Now, graphs G involve, either a single root cluster C_{ab} that contains both loops \mathcal{L}_a and \mathcal{L}_b , or two roots clusters C_a and C_b with \mathcal{L}_a in C_a and \mathcal{L}_b in C_b . The rules that define such graphs with n black clusters $\{C_i\}$ are identical to that of (4.22). In particular, the graphs are connected, and only permutations of black clusters C_i with identical numbers $N_i^{(p)}$ and $N_i^{(e)}$ are considered in the definition of symmetry factors. In (4.31), the measure and weights associated with root clusters are identical to that of black clusters, as in (4.30).

5 Physical interpretation of graphs G and concluding remarks

Expansion (4.29) is a reorganization of formal series (2.13) that is suitable for studying Coulomb gas at low fugacities and low temperatures, whether in a fully or partially ionized phase. Indeed, graphs in that expansion admit a natural interpretation in terms of the recombined entities and their mutual interactions, as discussed below.

- *Graphs with a single cluster*

First, we consider graph G_{N_p, N_e} with a single root cluster C_a . When fugacities go to zero, ϕ reduces to V , and we can replace all ring factors $\exp(I_R)$ by 1 and all Mayer coefficients \mathcal{B}_ϕ^T by \mathcal{B}^T , in $Z_\phi^T(C_a)$. Then, integration over all internal states of C_a reduces, after applying backwards Feynman-Kac formula, to the trace of a suitably truncated Mayer operator $[\exp(-\beta H_{N_p, N_e})]_{\text{Mayer}}^T$. For $G_{1,1}$ shown in Fig.13a, using expression (4.7) of $\mathcal{B}_{\phi,2}^T$, we find

$$\begin{aligned} [\exp(-\beta H_{1,1})]_{\text{Mayer}}^T &= \exp(-\beta H_{1,1}) - \exp(-\beta H_{1,1}^{(0)}) \\ &\quad + \int_0^\beta d\tau_1 \exp[-(\beta - \tau_1)H_{1,1}^{(0)}] V_{1,1} \exp[-\tau_1 H_{1,1}^{(0)}] \\ &\quad - \int_0^\beta d\tau_1 \int_0^{\tau_1} d\tau_2 \exp[-(\beta - \tau_1)H_{1,1}^{(0)}] V_{1,1} \exp[-(\tau_1 - \tau_2)H_{1,1}^{(0)}] V_{1,1} \exp[-\tau_2 H_{1,1}^{(0)}] \\ &\quad + \int_0^\beta d\tau_1 \int_0^{\tau_1} d\tau_2 \int_0^{\tau_2} d\tau_3 \exp[-(\beta - \tau_1)H_{1,1}^{(0)}] V_{1,1} \exp[-(\tau_1 - \tau_2)H_{1,1}^{(0)}] \\ &\quad \quad \quad \times V_{1,1} \exp[-(\tau_2 - \tau_3)H_{1,1}^{(0)}] V_{1,1} \exp[-\tau_3 H_{1,1}^{(0)}], \end{aligned} \quad (5.1)$$

where $H_{1,1}^{(0)} = H_{1,0} + H_{0,1}$ is the kinetic part of $H_{1,1}$, while $V_{1,1}$ is its potential part. Similar expressions for $[\exp(-\beta H_{N_p, N_e})]_{\text{Mayer}}^T$ can be obtained from the definition of $\mathcal{B}_{\phi, N}^T$ (see Section 4.2). In the resulting truncated structure analogous to (5.1), each Gibbs factor is associated with a complete Hamiltonian H_{M_p, M_e} ($M_p \leq N_p$ and $M_e \leq N_e$) that does incorporate any pair interactions between M_p protons and M_e electrons. At low fugacities, the leading contribution of G_{N_p, N_e} to $B_{N_p, N_e}^{(R)}$ then reads

$$\frac{1}{\Lambda} \text{Tr} [\exp(-\beta H_{N_p, N_e})]_{\text{Mayer}}^T. \quad (5.2)$$

Truncation in $[\exp(-\beta H_{N_p, N_e})]_{\text{Mayer}}^T$, inherited from that in the \mathcal{B}^T 's, ensures that trace (5.2) is finite contrary to that of $[\exp(-\beta H_{N_p, N_e})]_{\text{Mayer}}$ defining B_{N_p, N_e} : when it is expressed in position and spin spaces, matrix elements of $[\exp(-\beta H_{N_p, N_e})]_{\text{Mayer}}^T$ are integrable for any spatial configuration, i.e. their decay is sufficiently fast with respect to any

large particle separation. Moreover, that trace is correctly symmetrized with respect to Fermi statistics as a direct consequence of summation \sum_{Q_p, Q_e} in $\mathcal{D}(C_a)$ over all possible distribution of particles into loops.

According to the above properties, trace (5.2) does account for recombination into complex entities. Indeed, when temperature goes to zero, Gibbs operators associated with H_{M_p, M_e} provide exponentially growing terms arising from possible bound states with negative ground state energies $E_{M_p, M_e}^{(0)}$. Single term ($M_p = N_p, M_e = N_e$) can be interpreted as the ideal contribution, of the possible complex entity made of N_p protons and N_e electrons, while product of terms ($M_p < N_p, M_e < N_e$) describe its dissociation into several entities. Ideal contributions associated with familiar entities can be singled out in various graphs. For instance, $G_{1,1}$ shown in Fig.13a provides the ideal contribution

$$4z_p z_e [(m_p + m_e)/(2\pi\beta\hbar^2)]^{3/2} \exp(-\beta E_H), \quad (5.3)$$

of atoms H in their groundstate, or $G_{2,2}$ shown in Fig.13b provides the ideal contribution

$$2z_p^2 z_e^2 [(2m_p + 2m_e)/(2\pi\beta\hbar^2)]^{3/2} \exp(-\beta E_{H_2}) \quad (5.4)$$

of molecules H_2 in their groundstate with energy $E_{H_2} = E_{2,2}^{(0)}$. Notice that trace (5.2) appears as the natural $(N_p + N_e)$ -extension of the so-called second virial coefficient first introduced by Ebeling [2] for $N_p = N_e = 1$ (in that latter case, leading behaviour (5.3) of (5.2) can be readily inferred from perturbative low-temperature expansions [3]).

If leading contributions to the present graph G_{N_p, N_e} arise from simple or complex entities in their ground state with bare interactions, next corrections involve thermal excitations and collective effects. For instance, in $G_{2,2}$, corrections to (5.4) arise from excited states of molecule H_2 , as well as from thermal dissociation into atoms H , ions H_2^+ and H^- , protons and electrons. First corrections due to screening are obtained by expanding, in $Z_\phi^T(C_a)$, all ring factors $\exp(I_R)$ in powers of I_R and all Mayer coefficients \mathcal{B}_ϕ^T in powers of $\beta(\phi - V)$ (both I_R and $\beta(\phi - V)$ go to zero in a sufficiently dilute regime). At finite fugacities, non-perturbative collective effects like pressure dissociation, are accounted for in \mathcal{B}_ϕ^T . Since ϕ decays faster than the Coulomb potential, excited bound states with typical sizes larger than the screening length disappear: for instance, Rydberg states of atom H with principal quantum number n , are removed from contribution of $G_{1,1}$ (see Fig.13a) for $n^2 a_B > \kappa^{-1}$. Moreover, spectral broadening of energy levels in vacuum, directly follows from double-time dependence of $\phi(\mathcal{L}_i, \mathcal{L}_j)$ in s_i and s_j (any line element of \mathcal{L}_i interacts with any line element of \mathcal{L}_j). Since the equal-time condition that defines V (see (3.10)) no longer holds for ϕ [20], functional integration of \mathcal{B}_ϕ^T cannot be expressed in terms of an effective Hamiltonian. This is a particular manifestation of a general property regarding the motion of quantum particles coupled to a thermalized bath [34].

- *Graphs with two clusters and more*

According to the previous analysis, a particle cluster $C(N_p, N_e)$ can be associated with a possible complex entity made with N_p protons and N_e electrons. Therefore, a graph G with several clusters describes interactions between such entities. We consider successively various contributions arising from bonds $\mathcal{F}_\phi(C_i, C_j)$ between either neutral or charged particle clusters C_i and C_j .

Let us consider two neutral clusters C_i and C_j (numbers of protons and electrons in each given cluster are identical). Even if screening is incorporated into $\Phi(C_i, C_j)$, at sufficiently low fugacities $\Phi(C_i, C_j)$ can be replaced by the bare interaction between neutral clusters.

Indeed, like ϕ itself, that interaction displays a dipolar structure at large distances, and its contributions to G remain integrable. For instance, in graph $G_{2,2}$ shown in Fig.13c, collective effects in $Z_\phi^T(C_a)$, $Z_\phi^T(C_1)$ and $\Phi(C_a, C_1)$ can be neglected in a sufficiently dilute regime: the corresponding leading contribution accounts for familiar van der Waals interactions between two atoms H .

Now we turn to a neutral cluster C_i connected to a charged cluster C_j by a bond $\beta^2\Phi^2/2!$ or $-\beta^3\Phi^3/3!$. At sufficiently low fugacities, $\Phi(C_i, C_j)$ can be replaced, by the bare dipole-charge interaction between C_i and C_j , the square or cube of which is indeed integrable at large distances. For instance in graph $G_{2,3}$ shown in Fig.13d, leading contribution describes polarization effects of an atom H submitted to the electric field created by an ion H^- . In a bond $-\beta\Phi$, screening is *a priori* crucial for ensuring integrability (however, for some graphs sufficiently connected, leading contributions can still be estimated by keeping only bare interactions).

Eventually, we consider pairs (C_i, C_j) of charged clusters with a connecting bond $\mathcal{F}_\phi(C_i, C_j)$. Effective interaction $\Phi(C_i, C_j)$ in each bond takes into account screening due to free protons and free electrons at a mean-field level. Suitable combinations of charged pairs and bonds in G , provide contributions that account for various mechanisms. For instance, graph $G_{2,1}$ shown in Fig.13e gives screened contributions beyond mean-field Debye-like terms. Graph $G_{4,1}$ shown in Fig.13f describes modification of screened interactions between free protons due to the presence of ions H_2^+ . Summation of all similar graphs with convolution chains $(-\beta\Phi)*(-\beta\Phi)*\dots*(-\beta\Phi)$ and intermediate charged complex entities, allows us to introduce effective interactions screened by all charges present in the medium. Polarization of charged complex entities by other charges also appear. Graph $G_{3,1}$ shown in Fig.13g incorporates polarization effects of an ion H_2^+ by a free proton which is itself screened over distances of order κ^{-1} .

Thus, screened cluster expansion (4.22) provides a complete framework that sustains the so-called chemical picture at sufficiently low temperatures and low densities. Any complex entity made with N_p protons and N_e electrons can be associated with a particle cluster $C(N_p, N_e)$, while both ideal and interaction contributions are incorporated into statistical weights $Z_\phi^T(C)$ and bonds \mathcal{F}_ϕ . Every physical mechanism (see examples above) is described by a well behaved graph G , and consequently it can be estimated in a perfectly controlled and unambiguous way. We stress that screened cluster expansions (4.22), (4.30), (4.31) can be extended to any quantum nucleo-electronic plasma. Then particle clusters are made with any kind of nuclei and electrons, while statistical weights and bonds account for specific masses, charges and spins of all nuclei species. All topological and combinatorial rules that define graphs G , remain unchanged. Usefulness of screened cluster formalism for studying partially ionized gases is illustrated by various applications as described below.

It has been rigorously shown [35, 36] that the equation of state of the Hydrogen plasma reduces to that of an ideal mixture of protons, electrons, and atoms H in their ground state, in some suitable zero-temperature scaling limit defining the so-called Saha regime. The first rigorous result on the atomic limit has been established by Fefferman [37] (for a review, see [22]). Screened cluster expansions allow us to recover immediately ideal terms associated with free protons, free electrons and atoms H . All other contributions are shown to decay exponentially faster in the Saha regime. For instance, the ideal contribution (5.4) of molecules H_2 is smaller than (5.3) by factor $\exp[\beta(2\mu + E_H - E_{H_2})] \sim \exp[\beta(3E_H - E_{H_2})]$ (for μ close to E_H), which indeed exponentially vanishes at zero temperature since $3E_H < E_{H_2}$: though molecule H_2 is more stable than two atoms H ($E_{H_2} < 2E_H$), entropy dissociation overcomes energy minimization in the present very dilute regime. Moreover,

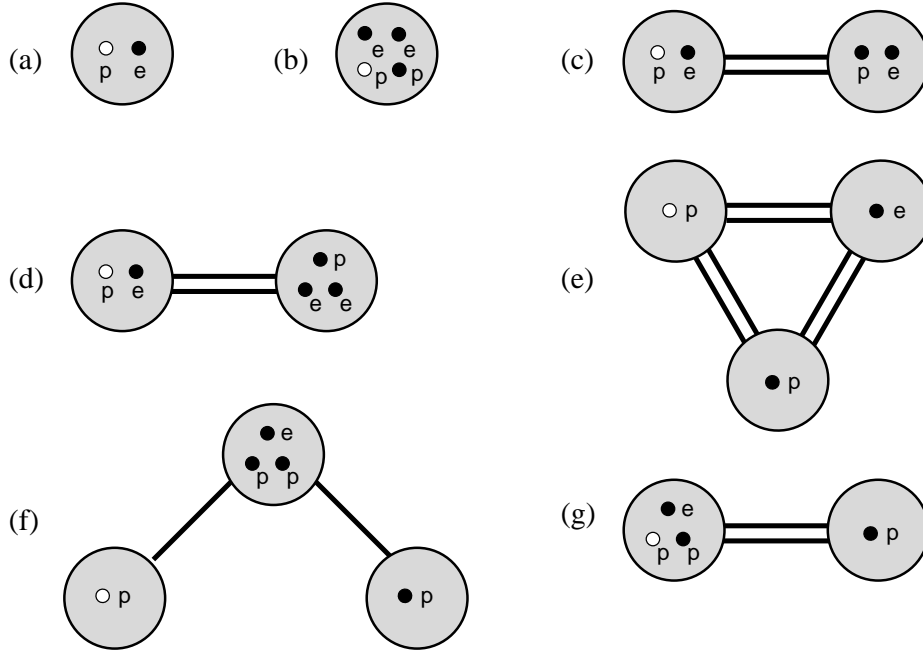


Fig. 13 – Examples of graphs G describing various physical effects. Formation of bound states: (a) hydrogen atom (b) hydrogen molecule H_2 ; (c) van der Waals interactions between two H atoms; (d) polarization of atom H by the field of a H^- ion; (e) contribution beyond mean-field to the screened interactions between two free (ionized) protons and a free electron; (f) modification of the screened interaction between two free protons due to a H_2^+ ion; (g) polarization of an ion H_2^+ by the field of a free proton screened over distances of order κ^{-1} .

detailed analysis of graphs G provide exact estimations of various corrections to ideal leading terms at finite (low) temperature and density. Such corrections arise from excited bound states of atoms H , thermal and entropy dissociation, recombination into other complex entities (H_2 , H_2^+ , H^- , ...), screening, interactions between entities, diffraction and exchange (all entities behave as almost classical particles). Those results will be published elsewhere [23].

For the Hydrogen plasma in Saha regime, particle correlations have been determined [25] by using screened cluster expansion (4.31). That analysis leads to the introduction of effective interactions between any entity, which all decay as $1/r^6$ at large relative distances r . In particular, familiar van der Waals forces between atoms H do appear. At zero temperature, standard perturbation formula for two atoms in the vacuum is exactly recovered. Corrections to that formula due to excited states and screening, are also calculated at finite temperature and density.

The dielectric response of the Hydrogen plasma in its atomic phase has been investigated with screened cluster formalism [38, 24]. That phase is defined within previous Fefferman limit [37] where μ is chosen slightly larger than E_H : it reduces to an ideal mixture of atoms H in their groundstate (such phase may also be viewed as a particular Saha regime where the fraction of ionized protons and electrons is arbitrarily small). The behaviour of wavenumber-dependent dielectric constant is analyzed by using expansion (4.31) in linear response to an infinitesimal external charge. A cross-over phenomenon

emerges, from a dielectric behaviour at wavenumbers much larger than κ , to a conductive behaviour at scales smaller than κ . Conductive behaviour is due to a finite tiny amount of free charges that are always present at finite temperature and density (here, screening length κ^{-1} is much larger than the mean distance between atoms H). The large plateau observed at scales larger than κ , leads to a natural definition of the (finite) dielectric constant for the atomic phase, independently of the presence of residual free charges. At zero temperature, the usual expression in terms of the polarizability of a single atom H is then exactly recovered.

Previous examples confirm that screened cluster formalism is well suited for studying dilute regimes at low temperature. This concerns both conceptual problems for Coulomb matter, like the existence of van der Waals forces at finite temperature and finite density or the definition of a dielectric regime, and also derivation of exact asymptotic expressions for equilibrium quantities. All those various analysis can be applied to any partially ionized (even neutral) gas. In addition, screened cluster expansions provide a promising route for deriving either approximation schemes or effective models. Both schemes and models might reasonably describe regimes with higher temperature and density, where analytic estimations are no longer possible.

A Combinatorial properties of Mayer graphs

We derive various combinatorial properties for Mayer graphs which are used in the transformations described in Section 4. These properties are related to the following central observation. Let G be an unlabelled Mayer graph built with N internal points x , weights z and bonds f (for our purpose it is unnecessary to take explicitly into account the root points). Its contribution reads

$$\frac{1}{S(G)} \int [\prod dx z(x)]_G [\prod f]_G. \quad (\text{A.1})$$

where $S(G)$ is its symmetry factor, i.e. the number of permutations of the N internal points that leave unchanged the product of bonds $[\prod f_{ij}]_{G_{lab}}$ associated with a labelled diagram G_{lab} with the same topological structure as that of G . The number of different labelled diagrams G_{lab} is equal to $N!/S(G)$. Once all integrations over internal points (x_1, \dots, x_N) have been performed, all contributions from different labelled diagrams are identical. Thus, (A.1) can be rewritten as

$$\frac{1}{N!} \sum_{G_{lab}} \int \prod_{i=1}^N dx_i z_i [\prod f_{ij}]_{G_{lab}} \quad (\text{A.2})$$

where the sum runs over all different labelled diagrams G_{lab} with the given topological structure determined by G . The transformation of (A.1) into (A.2) allows us to derive several useful identities as described below.

- *Decomposition of bonds*

If bond f is decomposed into a sum, $f = g + h$, contribution (A.1) can be rewritten in terms of that of graphs G^* built with two kinds of bonds, g and h . Replacing each bond f_{ij} by $g_{ij} + h_{ij}$ into (A.2), we find a sum over labelled diagrams G_{lab}^* where the product of bonds reads $[\prod g_{kl}]_{G_{lab}^*}$ times $[\prod h_{mn}]_{G_{lab}^*}$. Obviously labelled diagrams G_{lab}^* do exhibit the topological properties of Mayer graphs: they are connected, and two points are

connected by at most one bond which is either g or h . All G_{lab}^* 's have different products $[\prod g_{kl}]_{G_{lab}^*} [\prod h_{mn}]_{G_{lab}^*}$. They can be distributed into different classes where each class is defined by an unlabelled graph G_α^* ($\alpha = a, b, \dots$). In each class, two different labelled diagrams G_{lab}^* can be inferred from each other by a permutation of labels of internal points, so there are $N!/S(G_\alpha^*)$ such different labelled diagrams G_{lab}^* which all provide the same contribution after integration over the x 's. Thus, we obtain

$$\frac{1}{S(G)} \int [\prod dxz(x)]_G [\prod f]_G = \sum_{G_\alpha^*} \frac{1}{S(G_\alpha^*)} \int [\prod dxz(x)]_{G_\alpha^*} [\prod g]_{G_\alpha^*} [\prod h]_{G_\alpha^*} \quad (\text{A.3})$$

where the sum runs over all different unlabelled Mayer graphs G_α^* built with two kinds of bonds g and h . Moreover $S(G_\alpha^*)$ is the usual symmetry factor defined as the number of permutations of internal points that leave the product $[\prod g_{kl}]_{G_{lab}^*} [\prod h_{mn}]_{G_{lab}^*}$ unchanged for any labelled diagram G_{lab}^* associated with G_α^* . The topological structures of graphs G_α^* are inherited from that of G : they only differ by number and position of bonds g and h . If we sum (A.3) over all possible Mayer graphs G , we then find the remarkable identity

$$\sum_G \frac{1}{S(G)} \int [\prod dxz(x)]_G [\prod f]_G = \sum_{G^*} \frac{1}{S(G^*)} \int [\prod dxz(x)]_{G^*} [\prod g]_{G^*} [\prod h]_{G^*} \quad (\text{A.4})$$

where both graphs G and G^* are built within the same Mayer prescriptions.

- *Decomposition of weights*

Similarly to (A.4), we can transform (A.1) when weight z is decomposed as $z = u + v$. Again in (A.2) we replace each z_i by $u_i + v_i$. Following the same lines as above, we obtain the identity

$$\sum_G \frac{1}{S(G)} \int [\prod dxz(x)]_G [\prod f]_G = \sum_{G^*} \frac{1}{S(G^*)} \int [\prod dx] [\prod u(x)]_{G^*} [\prod v(x)]_{G^*} [\prod f]_{G^*} \quad (\text{A.5})$$

where now Mayer graphs G^* are defined with two kinds of weights u and v (and one kind of bond f). The symmetry factor $S(G^*)$ is defined as the number of permutations of internal points that leave products of weights $[\prod u_i]_{G_{lab}^*}$, $[\prod v_j]_{G_{lab}^*}$ and bonds $[\prod f_{kl}]_{G_{lab}^*}$ separately unchanged. Notice that an identity analogous to (A.5) holds when the internal state of x is made of two components s and t , i.e. $dx = ds + dt$: $u(x)dx$ and $v(x)dx$ are merely replaced by $z(s)ds$ and $z(t)dt$ respectively in the r.h.s. of (A.5).

- *Resummations of internal structures*

Now, let us consider labelled diagrams G_{lab} associated with the following Mayer graph G . Weights can be either u or v , while bonds can be either g , h or $h^2/2!$. Two connected points with weights u are linked by a bond g . A point with weight v is either singly connected to a point with weight u via a bond $h^2/2!$, or is the intermediate point of a convolution $h * h$ (the extremal points of convolutions $h * h * \dots * h$ carry weights u). The formula analogous to that relating (A.1) to (A.2) reads here

$$\begin{aligned} & \frac{1}{S(G)} \int [\prod dx]_G [\prod u(x)]_G [\prod v(x)]_G [\prod g]_G [\prod h]_G [\prod h^2/2!]_G = \\ & \frac{1}{N!} \sum_{G_{lab}} \int \prod_{i=1}^N dx_i [\prod u_j]_{G_{lab}} [\prod v_k]_{G_{lab}} [\prod g_{lm}]_{G_{lab}} [\prod h_{np}]_{G_{lab}} [\prod h_{qr}^2/2!]_{G_{lab}}. \quad (\text{A.6}) \end{aligned}$$

Then, we define a partition of points x with weights u in terms of M clusters X , such that the subdiagram associated with X is connected via bonds g only. The set of clusters X is determined by the topological structure of the unlabelled graph G . Each cluster X_i contains N_i points x with weights u , so there remains $L = N - \sum_{i=1}^M N_i$ points x with weights v . There are $N!/(N_1!N_2!\dots N_M!L!M!)$ different partitions of N labelled points into M labelled clusters (X_1, X_2, \dots, X_M) and L labelled points with weights v . Such labelled clusters and points (weights v) together with bonds g and h , define a labelled diagram \mathcal{G}_{lab} . The corresponding $N!/(N_1!N_2!\dots N_M!L!M!)$ labelled diagrams \mathcal{G}_{lab} provide identical contributions in the r.h.s of (A.6). Their sum reduces to

$$\frac{1}{L!M!} \int \prod_{i=1}^M \left[\frac{\prod_{j=1}^{N_i} dx_j^{(i)} u(x_j^{(i)})}{N_i!} \prod g_{lm} \right]_{X_i} \prod_{k=1}^L dx_k v(x_k) \left[\prod h_{np} \right]_{\mathcal{G}_{lab}} \left[\prod h_{qr}^2/2! \right]_{\mathcal{G}_{lab}}. \quad (\text{A.7})$$

In (A.7), $[\prod h_{np}]_{\mathcal{G}_{lab}}$ is a product of convolution chains $h * h * \dots * h$, with intermediate points x_k (weight $v(x_k)$) and two ending points belonging either to the same cluster X_i or to two different clusters X_i and X_j . Moreover, in $[\prod h_{qr}^2/2!]_{\mathcal{G}_{lab}}$, each bond $h^2/2!$ connects a point x_k (weight $v(x_k)$) to a point belonging to a cluster X_i . Now, we can proceed to a further summation of contributions (A.7) which only differ by the points (inside clusters X_i) at the extremities of convolution chains $h * h * \dots * h$ or bonds $h^2/2!$. This obviously leads to the introduction of

$$H(X_i, x_k) = \sum_{j=1}^{N_i} h(x_j^{(i)}, x_k), \quad (\text{A.8})$$

so (A.6) can be rewritten as

$$\begin{aligned} & \frac{1}{\mathcal{S}(G)} \int \left[\prod dx \right]_G \left[\prod u(x) \right]_G \left[\prod v(x) \right]_G \left[\prod g \right]_G \left[\prod h \right]_G \left[\prod h^2/2 \right]_G = \\ & \frac{1}{L!M!} \sum_{\mathcal{G}_{lab}} \int \prod_{i=1}^M \left[\frac{\prod_{j=1}^{N_i} dx_j^{(i)} u(x_j^{(i)})}{N_i!} \prod g_{lm} \right]_{X_i} \prod_{k=1}^L dx_k v(x_k) \left[\prod H_{np} \right]_{\mathcal{G}_{lab}} \left[\prod H_{qr}^2/2! \right]_{\mathcal{G}_{lab}}. \end{aligned} \quad (\text{A.9})$$

In (A.9), $[\prod H_{np}]_{\mathcal{G}_{lab}}$ is the product of convolution chains $H * H * \dots * H$ (intermediate points x_k and $H(x_k, x_l) = h(x_k, x_l)$) that either are attached to one cluster X_i or connect two clusters X_i and X_j . Moreover, in $[\prod H_{qr}^2/2!]_{\mathcal{G}_{lab}}$, each bond $H^2/2!$ connects a point x_k to a cluster X_i . The sum runs over all labelled diagrams \mathcal{G}_{lab} with different products of weights and bonds, and the same topological structure defined by G . Identity (A.9) can be easily summed over all graphs G that determine the following set of labelled diagrams \mathcal{G}_{lab} : clusters X_i , points x_k , bonds H_{np} and $H_{qr}^2/2!$, are identical, but internal structures of clusters in terms of bonds g are different. Since combinatorial prefactors for each labelled diagram \mathcal{G}_{lab} are all identical, the sum over labelled diagrams of products (over $i = 1, \dots, M$) of internal weights $[\prod g_{lm}]_{X_i}$ reduces to the product (over $i = 1, \dots, M$) of sums of those weights over all possible internal structures. This provides for each cluster X_i the weight Z_i

$$Z_i = \frac{\prod_{j=1}^{N_i} u(x_j^{(i)})}{N_i!} \sum \left[\prod g_{lm} \right]_{X_i} \quad (\text{A.10})$$

where the sum runs over all different products of bonds g_{lm} connecting labelled points inside X_i , i.e. over all corresponding Mayer labelled diagrams built with N_i points $x_j^{(i)}$

and bonds g_{lm} . If we set

$$dX_i = \prod_{j=1}^{N_i} dx_j^{(i)}, \quad (\text{A.11})$$

we eventually find

$$\begin{aligned} & \sum_G \frac{1}{S(G)} \int [\prod dx]_G [\prod u(x)]_G [\prod v(x)]_G [\prod g]_G [\prod h]_G [\prod h^2/2]_G \\ &= \sum_{\mathcal{G}_{lab}} \frac{1}{L!M!} \int \prod_{i=1}^M dX_i Z(X_i) \prod_{k=1}^L dx_k v(x_k) [\prod H_{np}]_{\mathcal{G}_{lab}} [\prod H_{qr}^2/2!]_{\mathcal{G}_{lab}} \\ &= \sum_{\mathcal{G}} \frac{1}{S(\mathcal{G})} \int [\prod dX Z(X)]_{\mathcal{G}} [\prod dx v(x)]_{\mathcal{G}} [\prod H]_{\mathcal{G}} [\prod H^2/2!]_{\mathcal{G}} \end{aligned} \quad (\text{A.12})$$

where the last line follows by applying backwards the relation between unlabelled graphs and labelled diagrams. The permutations accounted for in $S(\mathcal{G})$ act separately on sets of labelled clusters (X_1, \dots, X_M) and labelled points (x_1, \dots, x_L) , while they keep invariant each specific product of weights or bonds (this implies that permuted clusters necessarily contain the same number of particles).

All present identities result from simple combinatorics rules on one hand, and from the topological invariance of Mayer graphs under the considered transformations on another hand. They apply for any kind of points x : usual points (without internal degrees of freedom), loops (extended objects), clusters (sets of entities). Results derived in Section 4 (and those recalled in Section 3.2) follow by successive applications or combinations of these identities.

Acknowledgment In April 2002, one of us (AA) took part to the conference "Liquid State Theory: from White Dwarfs to Colloids" in honour of Jean-Pierre Hansen, on the occasion of his 60th birthday. AA is deeply indebted to Jean-Pierre for his constant support since he met him as a student, attending his enthusiastic and pedagogical lectures. AA would like to dedicate that paper to Jean-Pierre, as a close friend. All authors acknowledge his inspired contributions to statistical mechanics of fluids, as well as his remarkable management of the Laboratory of Physics of the ENS Lyon.

References

- [1] T. Morita, Equation of state of high temperature plasma, *Prog. Theor. Phys.* **22**:757 (1959).
- [2] W. Ebeling, Statistische thermodynamik der gebundenen zustande in plasmen, *Ann.Phys. (Leipzig)* **19**:104 (1967).
- [3] W.D. Kraeft, D. Kremp, W. Ebeling, and G. Ropke, *Quantum statistics of charged particles* (Plenum Press, New York, 1986).
- [4] T. Kahlbaum, The quantum-diffraction term in the free energy for Coulomb plasma and the effective-potential approach, *J. Phys. IV* **10** (P5):455 (2000)

- [5] W. Ebeling, W.D. Kraeft and D. Kremp, *Theory of bound states and ionization equilibrium in plasmas and solids* (Akademie-Verlag, Berlin, 1976).
- [6] F.J. Rogers, Statistical mechanics of Coulomb gases of arbitrary charge, *Phys.Rev.A* **10**: 2441 (1974).
- [7] F.J. Rogers, in *The equation of state in astrophysics* (Cambridge University Press, Cambridge, England, 1994).
- [8] A.L. Fetter and J.D. Walecka, *Quantum theory of many particle systems* (McGraw-Hill, New York, 1971).
- [9] Ph.A. Martin and P. Rothen, *Many-body problems and quantum field theory* (Springer, Berlin, 2002).
- [10] E.W. Montroll and J.C. Ward, Quantum statistics of interacting particles: general theory and some remarks on properties of an electron gas, *Phys.Fluid.* **1**: 55 (1958)
- [11] H.E. DeWitt, Evaluation of the quantum-mechanical ring sum with Boltzmann statistics, *J.Math.Phys.* **3**: 1216 (1962); Statistical mechanics of high-temperature quantum plasmas beyond the ring approximation, *J.Math.Phys.* **7**: 616 (1967).
- [12] H.E. DeWitt, M. Schlanges, A.Y. Sakakura, and W.D. Kraeft, Low density expansion of the equation of state for a quantum electron-gas, *Phys.Lett.A* **197**: 326 (1995).
- [13] B. Simon, *Functional integration and quantum physics* (Academic, New York, 1979); L.S. Schulman, *Techniques and applications of path integration* (Wiley, New York, 1981); G. Roepstorff *Path integral approach to quantum physics* (Springer, Berlin, 1994).
- [14] J. Ginibre, Some applications of functional integration in statistical mechanics, in *Statistical Mechanics and Quantum Field Theory*, C. DeWitt and R. Stora, eds., Les Houches (Gordon and Breach, 1971).
- [15] F. Cornu, Correlations in quantum plasmas: I. Resummations in Mayer-like diagrammatics, *Phys.Rev.E* **53**: 4562 (1996).
- [16] A. Alastuey, F. Cornu, and A. Perez, Virial expansions for quantum Plasmas: diagrammatic resummations, *Phys.Rev.E* **49**: 1077 (1994).
- [17] J.E. Mayer, The theory of ionic solutions, *J.Chem.Phys.* **18**: 1426 (1950); E.E. Salpeter, On Mayer's theory of cluster expansions, *Ann.Phys. (New-York)* **5**: 183 (1958).
- [18] E. Meeron, Theory of potentials of average force and radial distribution functions in ionic solutions *J. Chem. Phys.* **28**:630-643 (1958); *Plasma Physics* (McGraw-Hill, New York, 1961).
- [19] R. Abe, Giant cluster expansion theory and its application to high temperature plasma *Prog. Theor. Phys.* **22**:213 (1959).
- [20] V. Ballenegger, Ph.A. Martin and A. Alastuey, Quantum Mayer graphs for Coulomb systems and the analog of the Debye potential, *J. Stat. Phys.* **108**:169-211 (2002).

- [21] A. Alastuey and A. Perez, Virial expansion of the equation of state of a quantum plasma, *Europhys.Lett.* **20**: 19 (1992); A. Alastuey, F. Cornu and A. Perez, Virial expansion for quantum plasmas: Maxwell-Boltzmann statistics, *Phys.Rev.E* **51**: 1725 (1995); A. Alastuey and A. Perez, Virial expansion for quantum plasmas: Fermi-Bose statistics, *Phys.Rev.E* **53**: 5714 (1996); F. Cornu, Quantum plasmas with or without magnetic field. II. Exact low-density free energy, *Phys.Rev.E* **58**: 5293 (1998).
- [22] D.C. Brydges and Ph. A. Martin, Coulomb systems at low density: a review, *J. Stat. Phys.* **96**:1163-1330 (1999).
- [23] A. Alastuey, V. Ballenegger, F. Cornu and Ph.A. Martin, Equation of state of the Hydrogen Plasma in the atomic limit: estimations of non-ideal contributions at low temperature, *in preparation*.
- [24] V. Ballenegger and Ph.A. Martin, Quantum Coulomb systems: some exact results in the atomic limit, *Physica A* **306**:59-67 (2002); V. Ballenegger and Ph.A. Martin, Dielectric versus conductive behaviour in quantum gases: exact results for the hydrogen plasma, *in preparation*.
- [25] A. Alastuey, F. Cornu and Ph.A. Martin, Algebraic screening and van der Waals forces in partially ionized gases, in G. Kalman, K. Blagoev and J.J.M. Rommel (Eds.), *Strongly Coupled Coulomb Systems* (Plenum, New York, 1998); A. Alastuey, F. Cornu and Ph. A. Martin, Van der Waals forces at finite temperature and finite density, *in preparation*.
- [26] E.H. Lieb and J. Lebowitz, The constitution of matter: existence of thermodynamics for systems composed of electrons and nuclei, *Adv. Math.* **9**: 316-398 (1972).
- [27] F. Dyson and A. Lenard, Stability of matter I, *J. Math. Phys.* **8**:423-434 (1967); Stability of matter II, *J. Math. Phys.* **9**:698-711 (1968).
- [28] A. Alastuey and Ph. A. Martin, Absence of exponential clustering for static quantum correlations and time-displaced correlations in charged fluids, *Eur. Phys. Lett.* **6**:385-390 (1988); Absence of exponential clustering in quantum Coulomb fluids, *Phys. Rev. A* **40**:6485-6520 (1989).
- [29] F. Cornu and Ph.A. Martin, Electron gas beyond the random phase approximation: algebraic screening, *Phys.Rev.A* **44**: 4893 (1991).
- [30] F. Cornu, Correlations in quantum plasmas: II. Algebraic tails, *Phys.Rev.E* **53**: 4595 (1996); Exact algebraic tails of static correlations in quantum plasmas at low density, *Phys.Rev.Lett.* **78**: 1464 (1997); Quantum plasma with or without uniform magnetic field. III. Exact low-density algebraic tails of correlations *Phys.Rev.E* **58**: 5322 (1998).
- [31] J.P. Hansen and I.R. McDonald, *Theory of simple liquids* (Academic Press, London, 2nd edition, 1986).
- [32] F. Cornu, Quantum plasma with or without uniform magnetic field. I. General formalism and algebraic tails of correlations *Phys. Rev. E* **58**:5268-5292 (1998).
- [33] A. Alastuey and W. Appel, A model of relativistic one-component plasma with Darwin interactions, *Physica A* **238**: 369 (1997).

- [34] R.P. Feynman and A.R. Hibbs, *Quantum Mechanics and Path Integral* (McGraw-Hill, 1965).
- [35] J.G. Conlon, E.H. Lieb and H.T. Yau, The Coulomb gas at low temperature and low density, *Commun. Math. Phys.* **125**:153-180 (1989).
- [36] N. Macris and Ph.A. Martin, Ionization equilibrium in the proton-electron gas, *J. Stat. Phys.* **60**:619-637 (1990).
- [37] C. Fefferman, The atomic and molecular nature of matter, *Rev. Math. Iberoamericana* **1**:1-44 (1985).
- [38] V. Ballenegger, *Étude des phénomènes d'écran et de polarisation dans un plasma quantique par la méthode des graphes de Mayer*, (Ph.D.thesis, École Polytechnique Fédérale de Lausanne, 2002).